Supporting Information (SI)

The Influence of Stepwise P-Oxidation on the Coordination and Redox Behavior of W-bisphosalkyne Complex Ligands

Kai Helmdach, Alexander Villinger and Wolfram W. Seidel*

Institut für Chemie, Universität Rostock,

Albert-Einstein-Straße 3a, 18059 Rostock, Germany

1. Content

2. Crystallographic Details

Table S1. Crystallographic details for **1O**, **1S**, **2O**, **2OO** and **2SS**.

	1O	**1S**	**2O**	**2OO**	**2SS**
empirical formula	$C_{33}H_{39}BIN_6O_2PW{\cdot}C_5H_{12}$	$C_{33}H_{39}BIN_6OPSW{\cdot}1.5\ CH_2Cl_2$	$0.9[C_{45}H_{48}BIN_6O_2P_2W]{\cdot}0.1[C_{45}H_{48}BBrN_6O_2P_2W{\cdot}CH_2Cl_2]$	$C_{45}H_{48}BIN_6O_3P_2W{\cdot}CHCl_3$	$C_{45}H_{48}BIN_6OP_2S_2W{\cdot}CH_2Cl_2$
M_W / g·mol^{-1}	976.38	1047.68	1091.61	1223.76	1221.44
colour, habit	green, block	green, block	green, plate	orange, block	red, block
crystal system	orthorhombic	triclinic	monoclinic	triclinic	monoclinic
space group	$Pca2_1$	P-1	$P2_1/n$	P-1	$P2_1/c$
a / Å	17.3399(9)	9.7681(6)	10.9974(6)	11.0779(3)	12.9921(16)
b / Å	10.3826(6)	13.5347(9)	18.5870(11)	11.7986(3)	18.476(2)
c / Å	21.7550(12)	15.6453(9)	21.9383(13)	19.9114(5)	21.765(3)
α / °	90	99.294(3)	90	88.563(1)	90
β / °	90	91.660(3)	98.135(2)	81.797(1)	96.020(7)
γ / °	90	105.648(3)	90	70.936(1)	90
V / Å^3	3916.6(4)	1959.9(2)	4439.3(4)	2433.95(11)	5195.8(11)
Z	4	2	4	2	4
$\rho_{calcd.}$ / g·cm^{-1}	1.656	1.775	1.633	1.670	1.561
μ / mm^{-1}	3.819	4.070	3.453	3.284	3.101
$\lambda_{MoK\alpha}$ / Å	0.71073	0.71073	0.71073	0.71073	0.71073
T / K	123(2)	123(2)	123(2)	123(2)	123(2)
collected refl.	63826	65084	182355	78855	147369
unique refl.	14011	14191	14760	17534	18777
refl. $I > 2\sigma(I)$	12168	11988	11850	15092	16996
R_{int}	0.0494	0.0506	0.0786	0.0324	0.0411
parameters/restraints	418/5	489/3	576/36	593/24	595/61
R_1 [$I > 2\sigma$(I)]	0.0264	0.0344	0.0394	0.0382	0.0254
wR_2 (all data)	0.0595	0.0667	0.0745	0.0880	0.0632
GooF	0.912	1.044	1.027	1.046	1.018
resid. density [eÅ^{-3}]	0.981/–1.107	3.437/–1.880	1.427/–1.944	2.223/–3.238	2.283/–1.547
CCDC	1577105	1577104	1577111	1577106	1577110

Table S2. Crystallographic details for **3**, **3O**, **3S**, **4** and **5**-PF_6.

	3	**3O**	**3S**	**4**	**5-PF_6**
empirical formula	$C_{45}H_{48}BCl_2IN_6OP_2PdW\cdot 3\ CH_2Cl_2$	$C_{45}H_{48}BCl_2IN_6O_2P_2PdW\cdot 2\ CH_2Cl_2$	$C_{45}H_{48}BCl_2IN_6OP_2PdSW\cdot 3\ CH_2Cl_2$	$C_{39}H_{52}BI_3N_6OP_2PdW\cdot 1.69\ CH_2Cl_2$	$C_{90}H_{96}AuB_2F_6I_2N_{12}O_2P_5W_2\cdot 4.25\ CH_2Cl_2$
M_W / g·mol^{-1}	1504.47	1435.54	1536.53	1575.59	2847.29
colour, habit	red, block	green, plate	purple, plate	red, block	brown, plate
crystal system	monoclinic	monoclinic	monoclinic	monoclinic	triclinic
space group	$P2_1/n$	$P2_1/n$	$P2_1/n$	$C2/c$	P-1
a / Å	15.4833(7)	13.720(5)	18.351(5)	33.3306(10)	10.1419(4)
b / Å	16.6409(7)	19.126(6)	16.067(14)	18.8592(6)	14.2748(5)
c / Å	21.7609(9)	20.619(7)	19.509(5)	19.0257(6)	19.4576(7)
α / °	90	90	90	90	80.163(2)
β / °	91.775(3)	102.678(15)	92.406(12)	112.875(1)	83.571(2)
γ / °	90	90	90	90	77.328(2)
V / Å^3	5604.1(4)	5279(3)	5747(3)	11018.8(6)	2699.8(2)
Z	4	4	4	8	1
$\rho_{calcd.}$ / g·cm^{-1}	1.783	1.806	1.776	1.900	1.751
μ / mm^{-1}	3.403	3.511	3.355	4.355	4.398
$\lambda_{MoK\alpha}$ / Å	0.71073	0.71073	0.71073	0.71073	0.71073
T / K	123(2)	128(2)	123(2)	123(2)	173(2)
collected refl.	77468	194189	277848	71200	19960
unique refl.	16283	19874	19126	14641	19960
refl. $I > 2\sigma(I)$	8894	15927	14952	9183	15608
R_{int}	0.0318	0.0797	0.0756	0.0890	0.0497
parameters/restraints	651/21	649/6	654/6	583/16	702/138
R_1 [$I > 2\sigma(I)$]	0.0558	0.0405	0.0310	0.0471	0.0354
wR_2 (all data)	0.0990	0.0755	0.0627	0.1077	0.0817
GooF	1.001	1.084	1.040	1.016	1.032
resid. density [eÅ^{-3}]	1.266/–2.360	2.727/–2.145	0.980/–1.490	1.604/–1.715	1.236/–0.938
CCDC	1577102	1577103	1577108	1577109	1577107

3. Crystal Structure of 1S

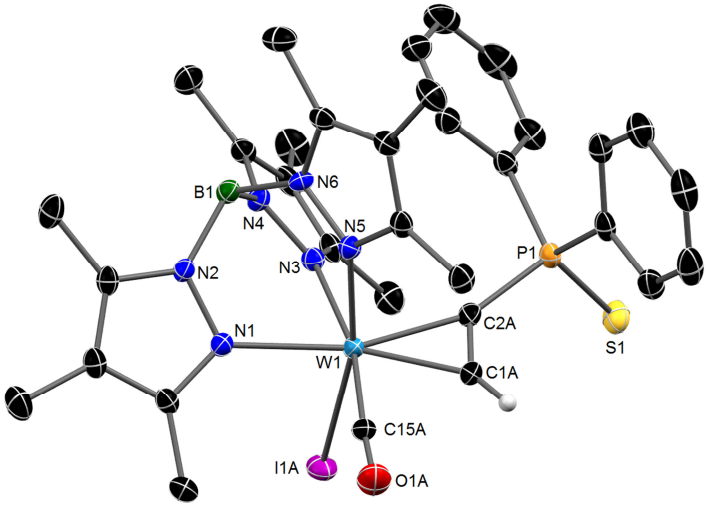

Figure S1. Molecular structure of **1S** in the crystal of **1S**·1.5 CH_2Cl_2 with thermal ellipsoids set at 50% probability. Hydrogen atoms and co-crystallized CH_2Cl_2 have been omitted for clarity. Major occupation is shown for the disordered alkyne-CO-I ligand set. Selected bond lengths [Å] and angles [°]: W1–I1A 2.7605(3), W1–N1 2.232(2), W1–N3 2.237(2), W1–N5 2.175(2), W1–C1A 2.031(3), W1–C2A 2.045(3), W1–C15A 1.959(4), C1A–C2A 1.312(5), C2A–P1 1.789(3), P1–S1 1.9573(10), P1–C2A–C1A 135.5(2).

4. Crystal Structure of 2OO

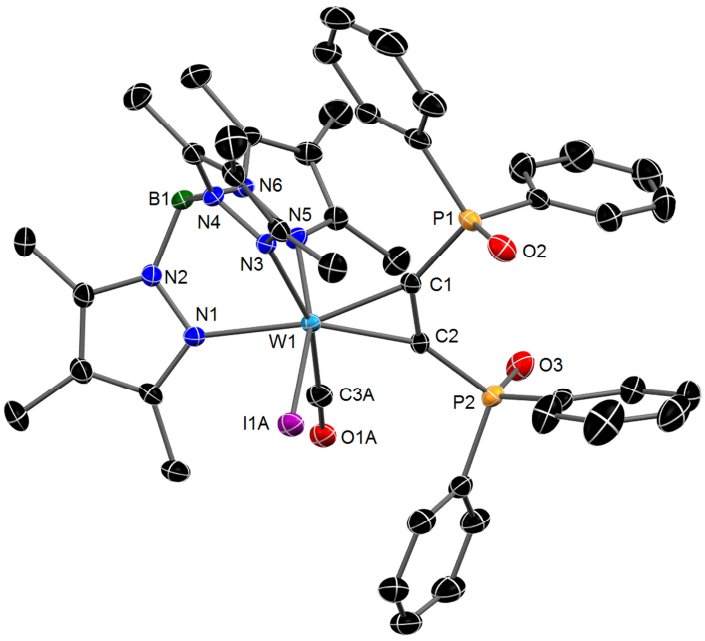

Figure S2. Molecular structure of **2OO** in the crystal of **2OO**·$CHCl_3$ with thermal ellipsoids set at 50% probability. Hydrogen atoms and co-crystallized $CHCl_3$ have been omitted for clarity. Major occupation is shown for the disordered iodide/carbonyl ligand set. Selected bond lengths [Å] and angles [°]: W1–I1A 2.7744(3), W1–N1 2.228(3), W1–N3 2.237(2), W1–N5 2.197(3), W1–C1 2.054(3), W1–C2 2.061(3), W1–C3A 1.970(4), C1–C2 1.333(4), C1–P1 1.803(3), C2–P2 1.805(3), P1–O2 1.483(3), P2–O3 1.490(3), P1–C1–C2 135.2(2), C1–C2–P2 138.7(2).

5. Crystal Structure of 4

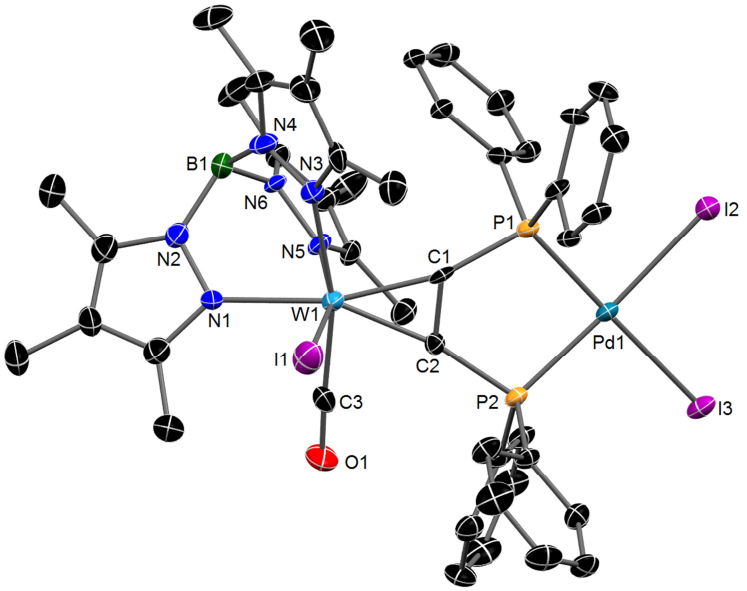

Figure S3. Molecular structure of **4** in the crystal of **4**·1.7 CH_2Cl_2 with thermal ellipsoids set at 50% probability. Hydrogen atoms and co-crystallized CH_2Cl_2 have been omitted for clarity. Selected bond lengths [Å] and angles [°]: W1–I1 2.7730(6), W1–N1 2.215(6), W1–N3 2.243(5), W1–N5 2.180(5), W1–C1 2.034(7), W1–C2 2.055(6), W1–C3 1.968(8), C1–C2 1.323(8), C1–P1 1.807(7), C2–P2 1.834(6), P1–Pd1 2.259(2), P2–Pd1 2.279(2), Pd1–I2 2.6334(7), Pd1–I3 2.6407(6), P1–C1–C2 118.3(5), C1–C2–P2 120.7(5), I2–Pd1–I3 91.59(2).

6. Orbital Interactions in d^4 Alkyne Carbonyl Complexes

The parallel alignment of the alkyne to the carbonyl ligand in d^4 metal complexes can be rationalized by optimized π-interactions between the d_{xy}, d_{xz} and d_{yz} orbitals and the respective ligand orbitals as shown in Figure S4 for Tp*W(CO)(I)(alkyne).[S1] Only in this arrangement the carbonyl can act as a twofold π-acid (d_{yz}→$CO\pi^*_y$ and d_{xz}→$CO\pi^*_x$) at the same time as the alkyne can act as both π-acid (d_{yz}→$CC\pi^*$) and π-base ($CC\pi_{\perp}$→d_{xy}) retaining its 4e donor character. Independent EHMO calculations by Templeton et al. and Connelly et al. support this rationale even when including any metal halide interactions in the picture.[S2]

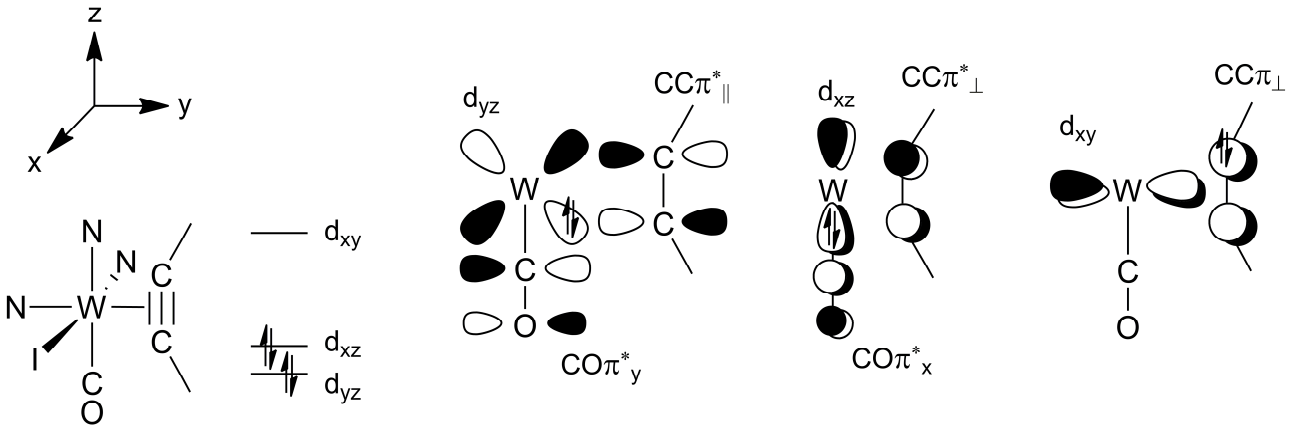

Figure S4. Schematic representation of important orbital interactions in Tp*W(CO)(I)(alkyne) and qualitative molecular orbital energies for a parallel alkyne-carbonyl arrangement adapted from reference S1.

7. Cyclic Voltammetry

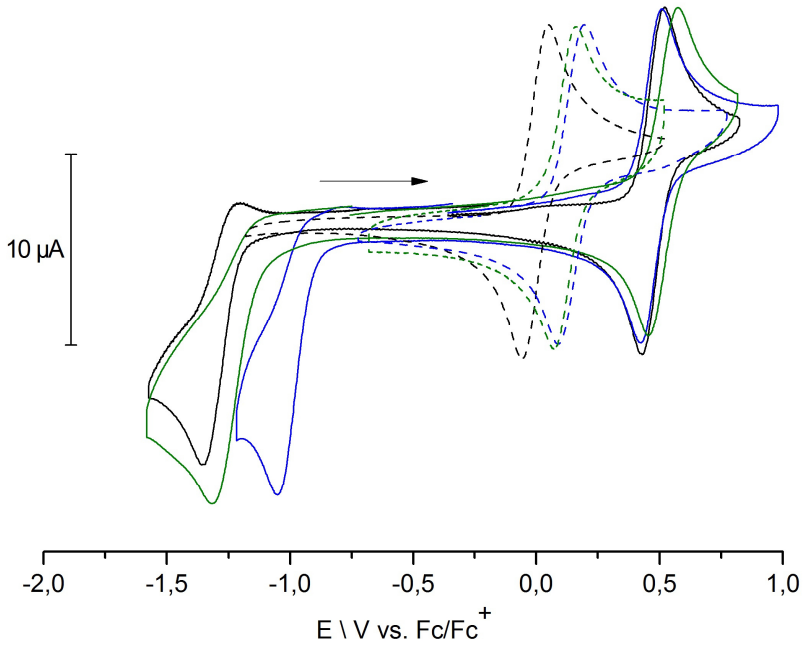

Figure S5. Selected cyclic voltammetry of W bisphosalkyne complexes (dashed lines) **2** (black), **2O** (blue), **2S** (green) and their respective $PdCl_2$ coordination compounds (solid lines) **3** (black), **3O** (blue) and **3S** (green) measured in CH_2Cl_2 comparing the reversible oxidation waves for the $W^{II/III}$ redox process and irreversible reduction of Pd^{II}.

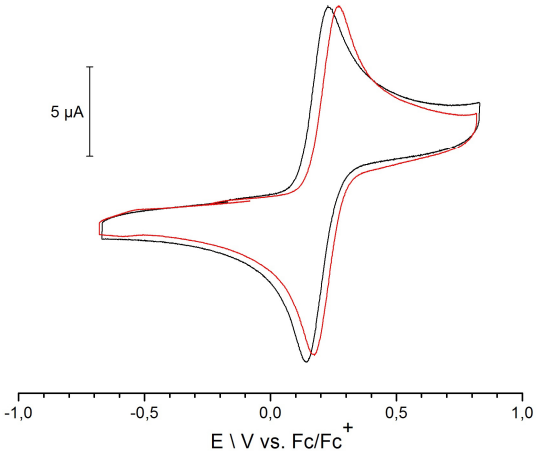

Figure S6. Selected cyclic voltammetry of bisphosalkyne complexes **2OO** (red) and **2SS** (black).

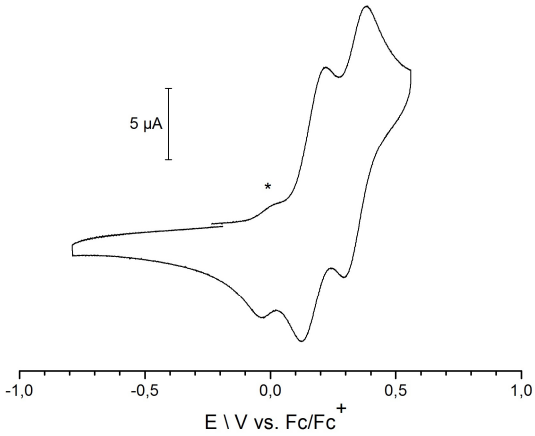

Figure S7. Selected cyclic voltammetry of trinuclear complexe **5**-PF_6.

* traces of **2**.

8. Stoichiometric Oxidation of 5-PF_6

To a solution of complex **5**-PF_6 (10 mg, 0,004 mmol) in CH_2Cl_2 (3 ml) was added a solution of $[\{C_5H_4C(O)CH_3\}Fe(C_5H_5)][PF_6]$[S3] (1,5 mg, 0,004 mmol) in CH_2Cl_2 (3 ml) in one portion. The light orange solution turned immediately red. IR spectroscopy (see Figure S8) indicated the formation of mononuclear $\mathbf{2}^+$ (2079 cm^{-1})[S4] and an unidentified species (1960 cm^{-1}). Further monitoring by IR spectroscopy showed that degeneration started within minutes resulting in regeneration of the starting complex $\mathbf{5}^+$ (1921 cm^{-1}). ^{31}P NMR spectroscopy confirmed the identity of **5**-PF_6 but did not allow the identification of other side-products due to their low concentrations. A plausible explanation for the reduction of $\mathbf{2}^+$ and regeneration of $\mathbf{5}^+$ is given in Figure S9 postulating the formation of tetranuclear $[Au_2(\mathbf{2})_2]^{2+}$ along with $\mathbf{2}^+$ upon oxidation. Disproportionation of $\mathbf{2}^+$ and reaction of **2** with Au_2W_2 recover 75 % of **5**-PF_6. However, the fate of the W(IV)-species and one Au(I) equivalent remains unknown. The observation of traces of the redox couple $\mathbf{2}/\mathbf{2}^+$ already in the cyclic voltammogram (Figure S7) supports the suggested reaction sequence.

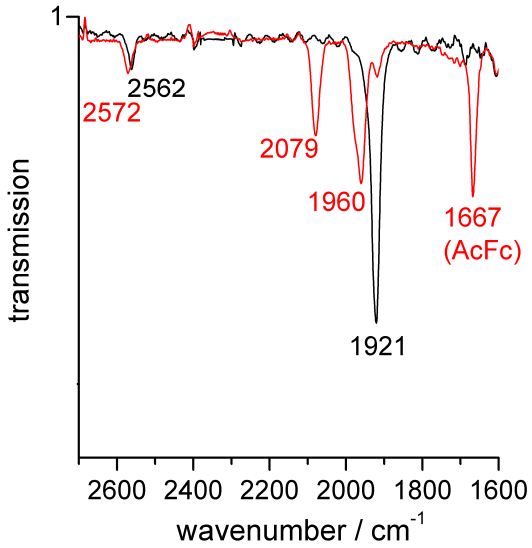

Figure S8. Selected IR spectra in CH_2Cl_2 solution of **5**-PF_6 (black line) and moments after addition of 1 equivalent $[AcFc][PF_6]$, AcFc = $\{C_5H_4C(O)CH_3\}Fe(C_5H_5)$ (red line).

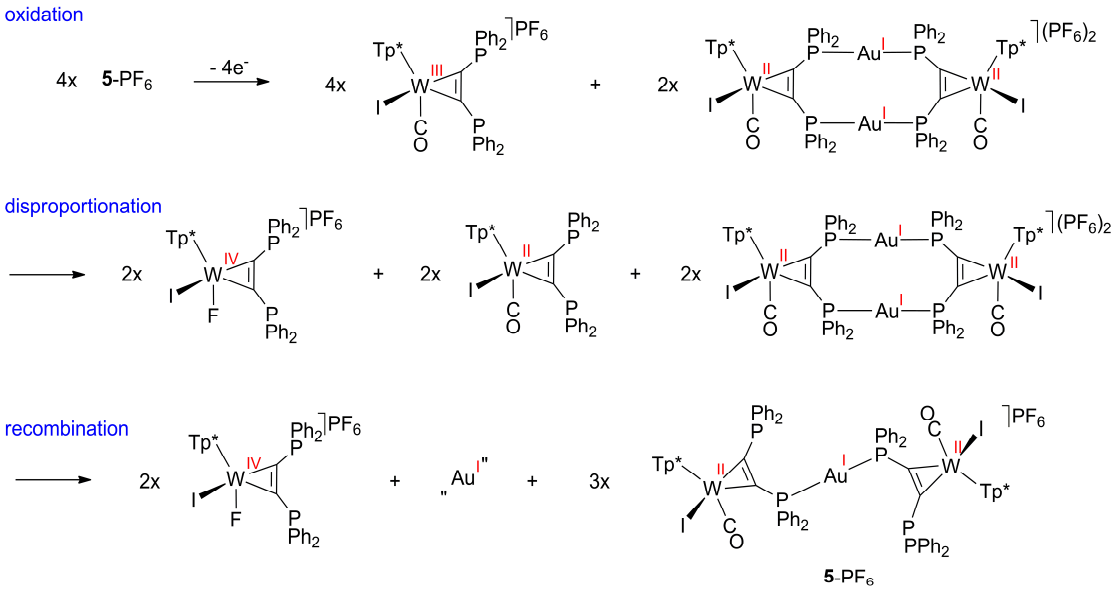

Figure S9. Plausible sequence for the oxidation of **5**-PF_6 and subsequent reactions. Tp* = $[(pz^{Me_3})_3BH]^-$

9. NMR Spectra

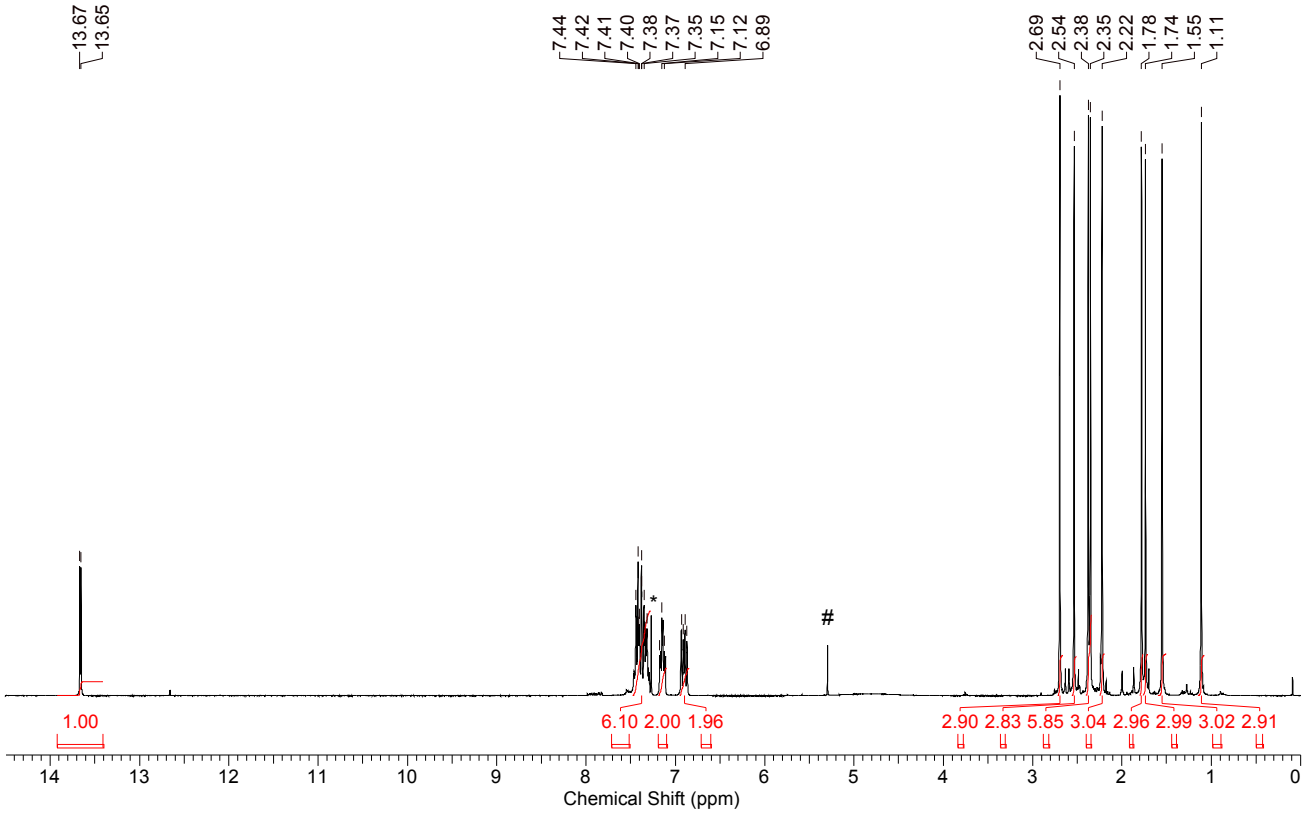

Figure S10. ^{1}H NMR of **1O** in $CDCl_3$ (*), # CH_2Cl_2.

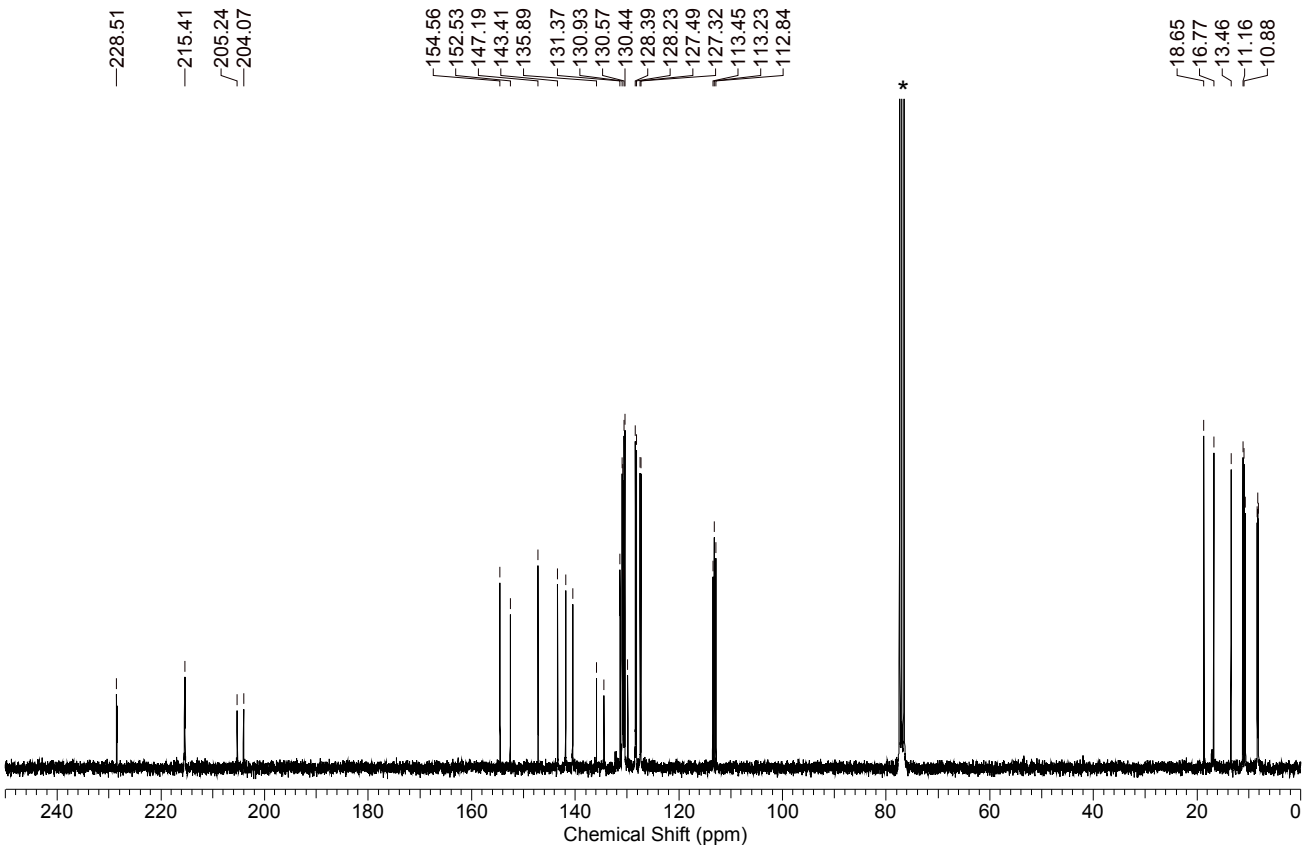

Figure S11. ^{13}C NMR of **1O** in $CDCl_3$ (*).

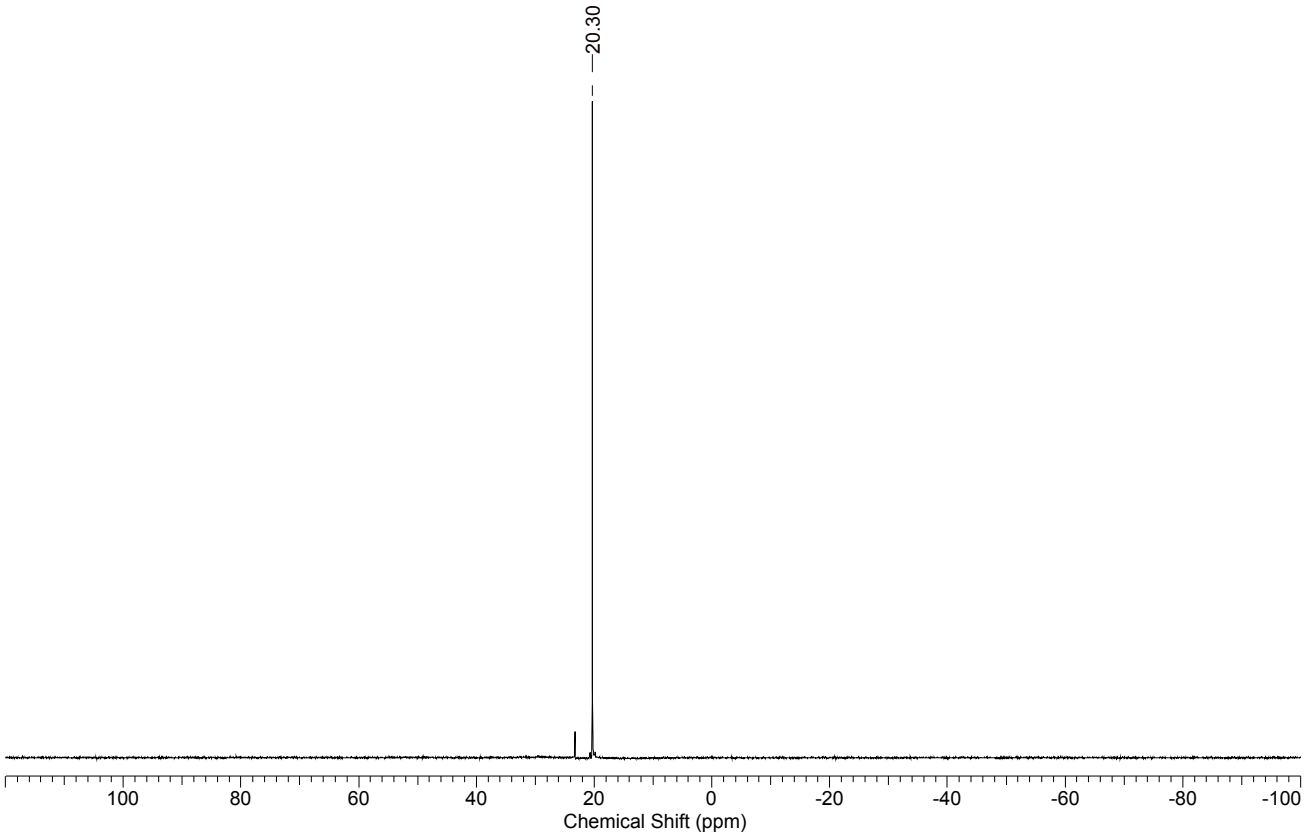

Figure S12. ^{31}P NMR of **1O** in $CDCl_3$.

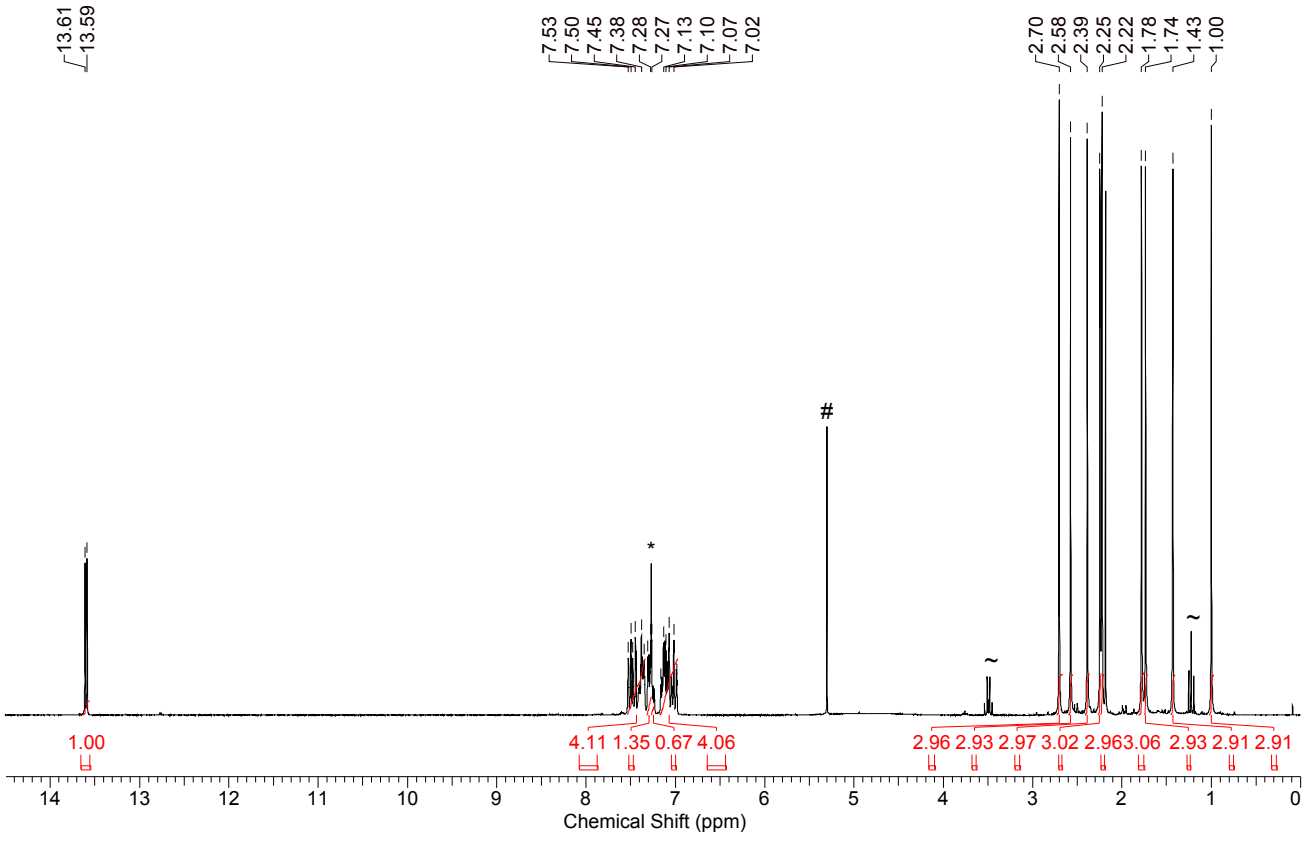

Figure S13. ^{1}H NMR of **1S** in $CDCl_3$ (*), # CH_2Cl_2, ~ diethyl ether.

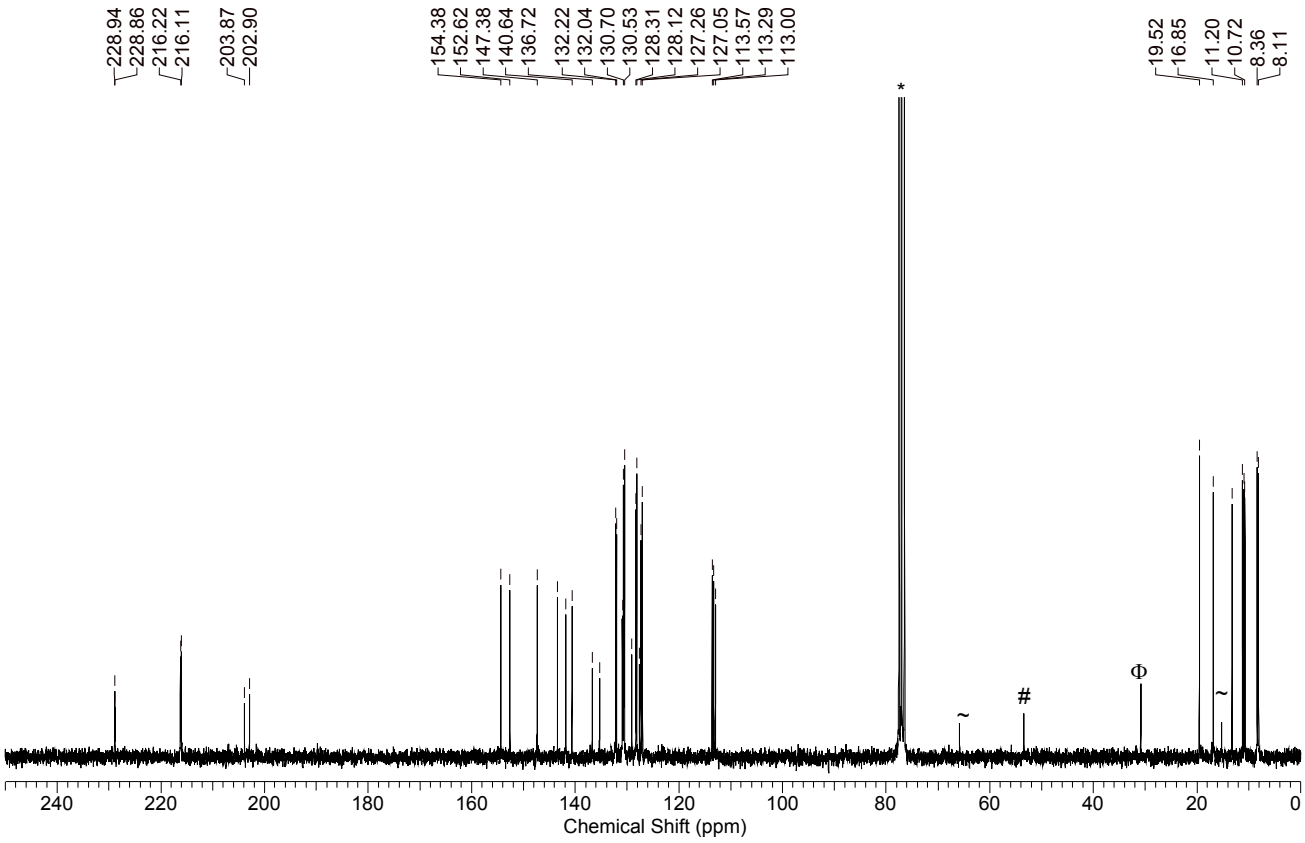

Figure S14. ^{13}C NMR of **1S** in $CDCl_3$ (*), # CH_2Cl_2, ~ diethyl ether, Φ acetone.

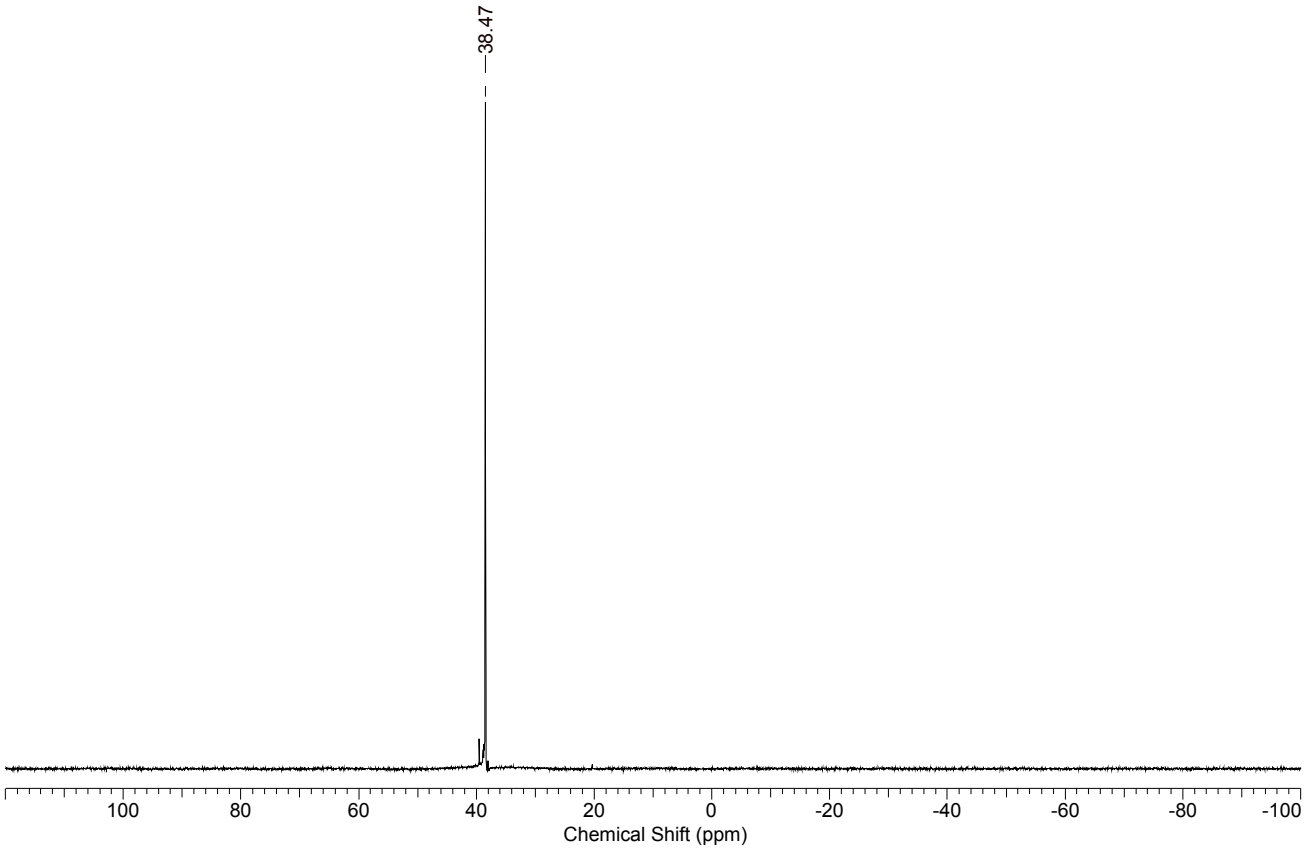

Figure S15. ^{31}P NMR of **1S** in $CDCl_3$.

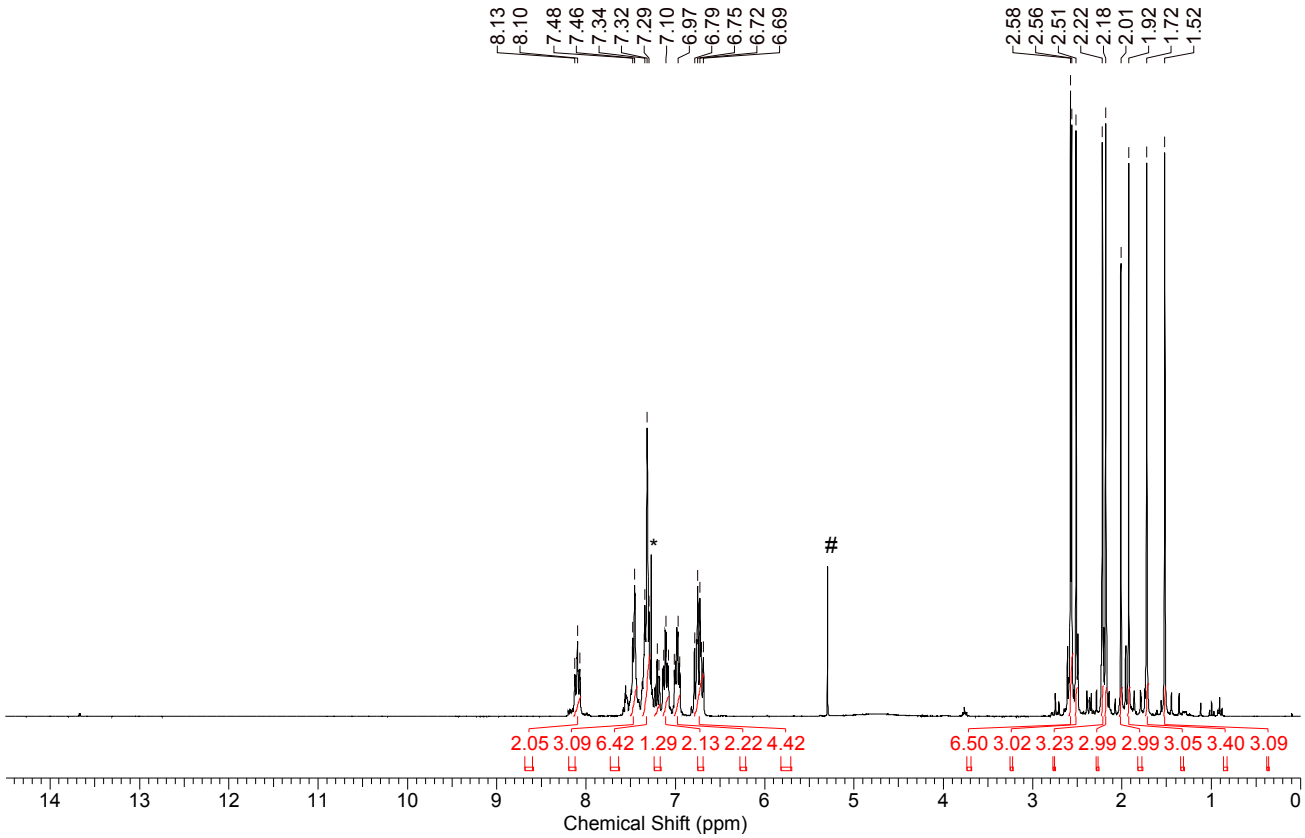

Figure S16. ^{1}H NMR of **2O** in $CDCl_3$ (*), # CH_2Cl_2.

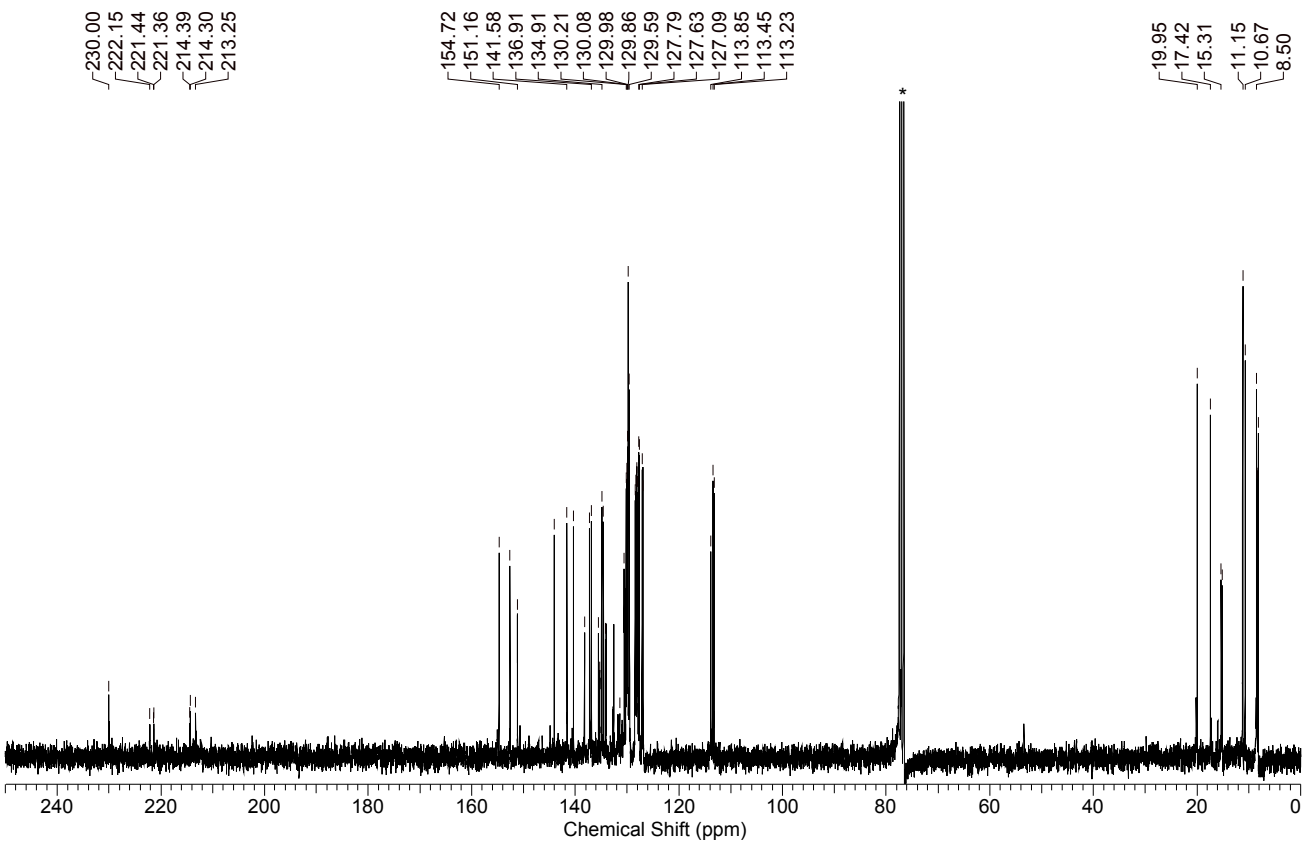

Figure S17. ^{13}C NMR of **2O** in $CDCl_3$ (*).

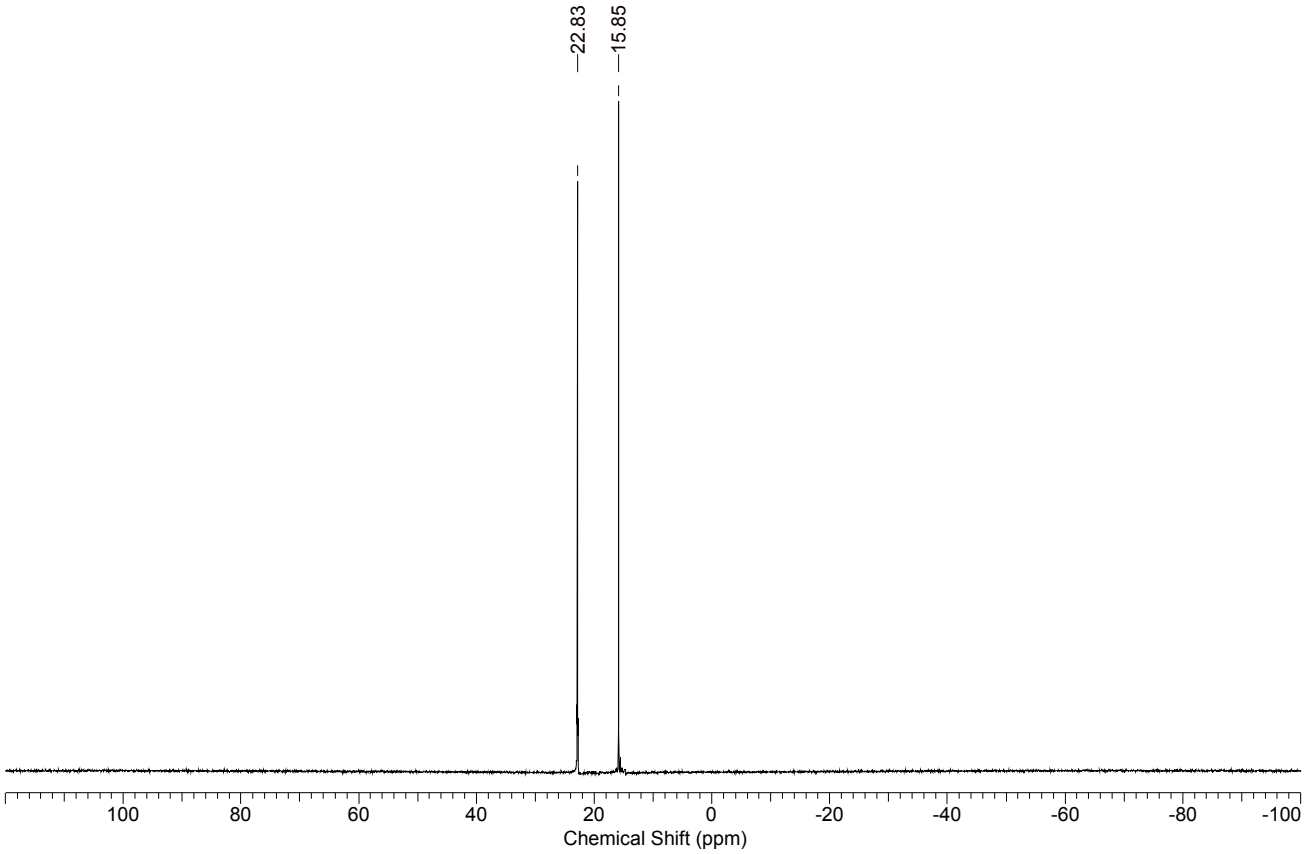

Figure S18. ^{31}P NMR of **2O** in $CDCl_3$.

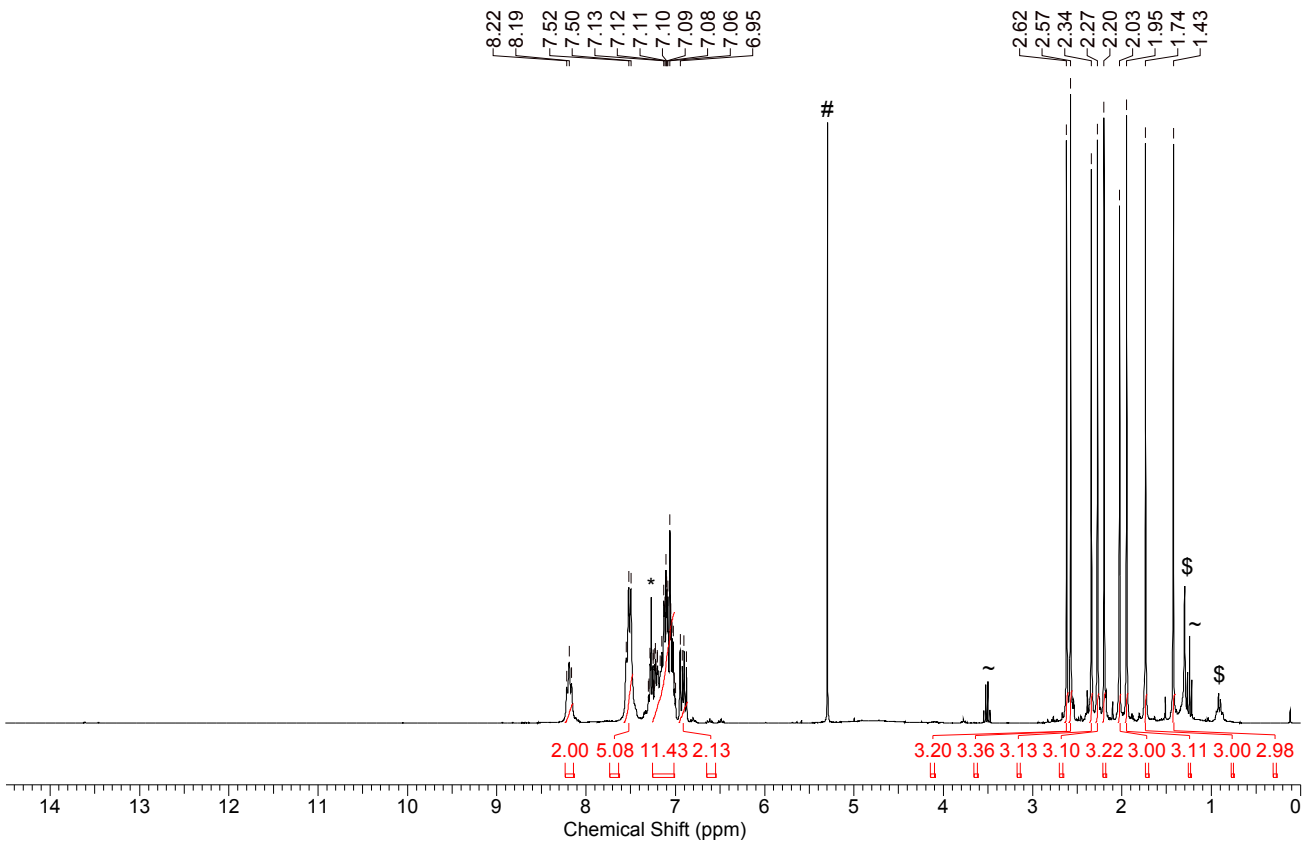

Figure S19. ^{1}H NMR of **2S** in $CDCl_3$ (*), # CH_2Cl_2, ~ diethyl ether, $ *n*-pentane.

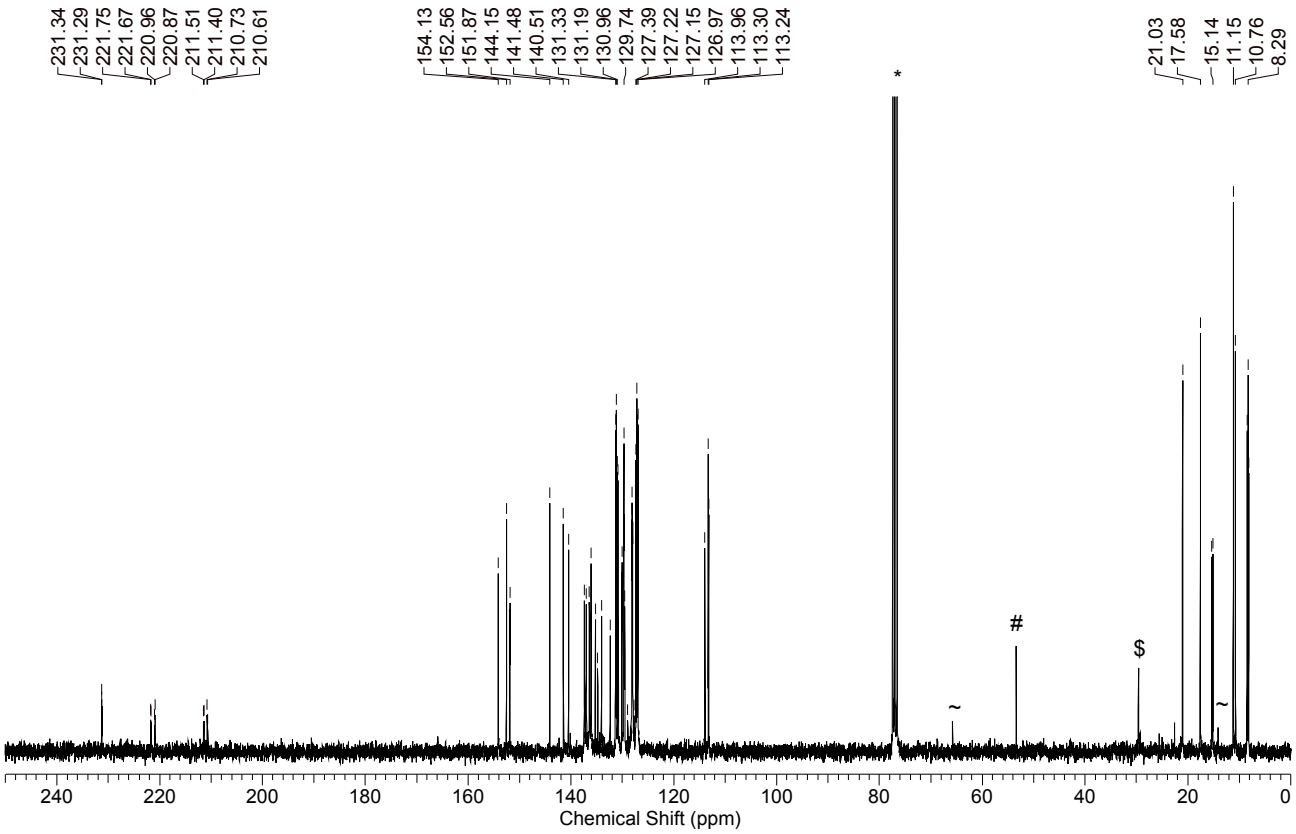

Figure S20. ^{13}C NMR of **2S** in $CDCl_3$ (*), # CH_2Cl_2, ~ diethyl ether, $ *n*-pentane.

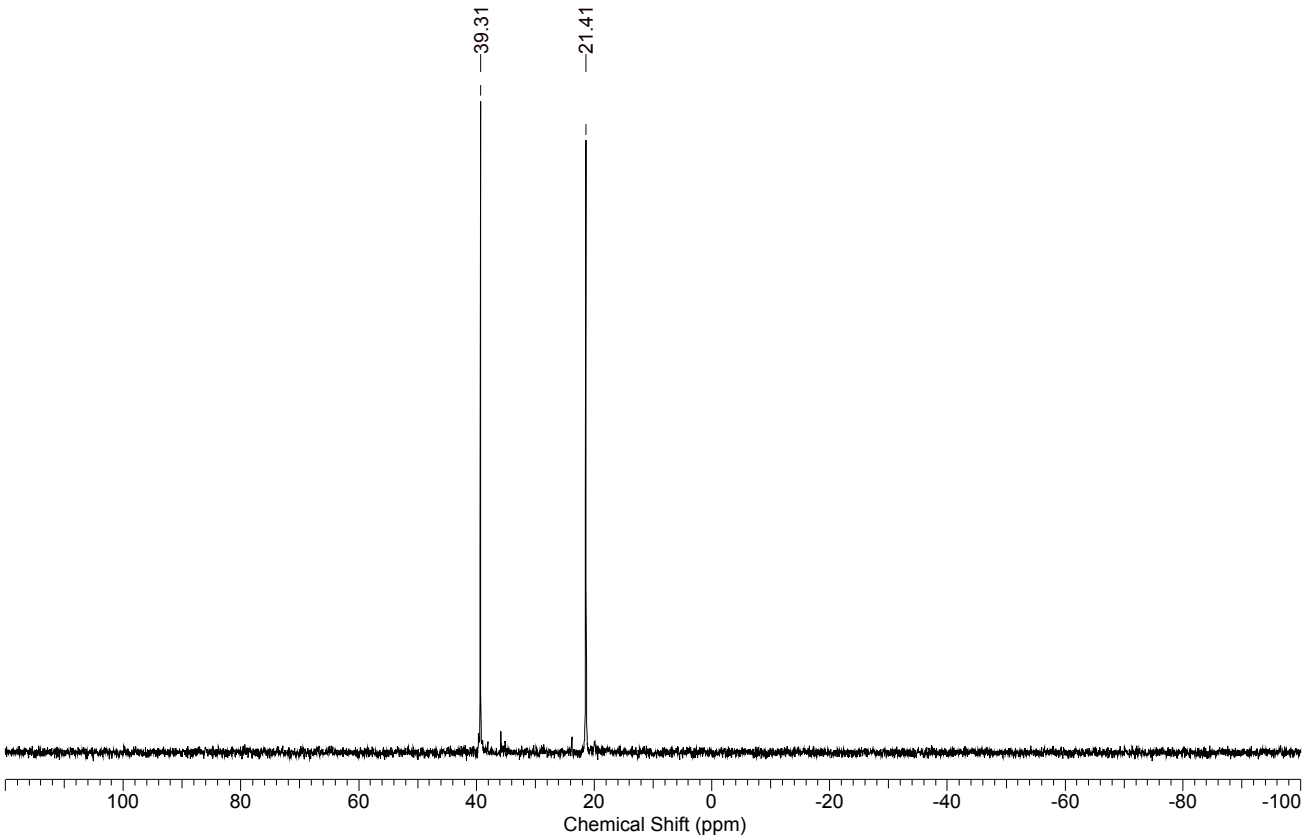

Figure S21. ^{31}P NMR of **2S** in $CDCl_3$.

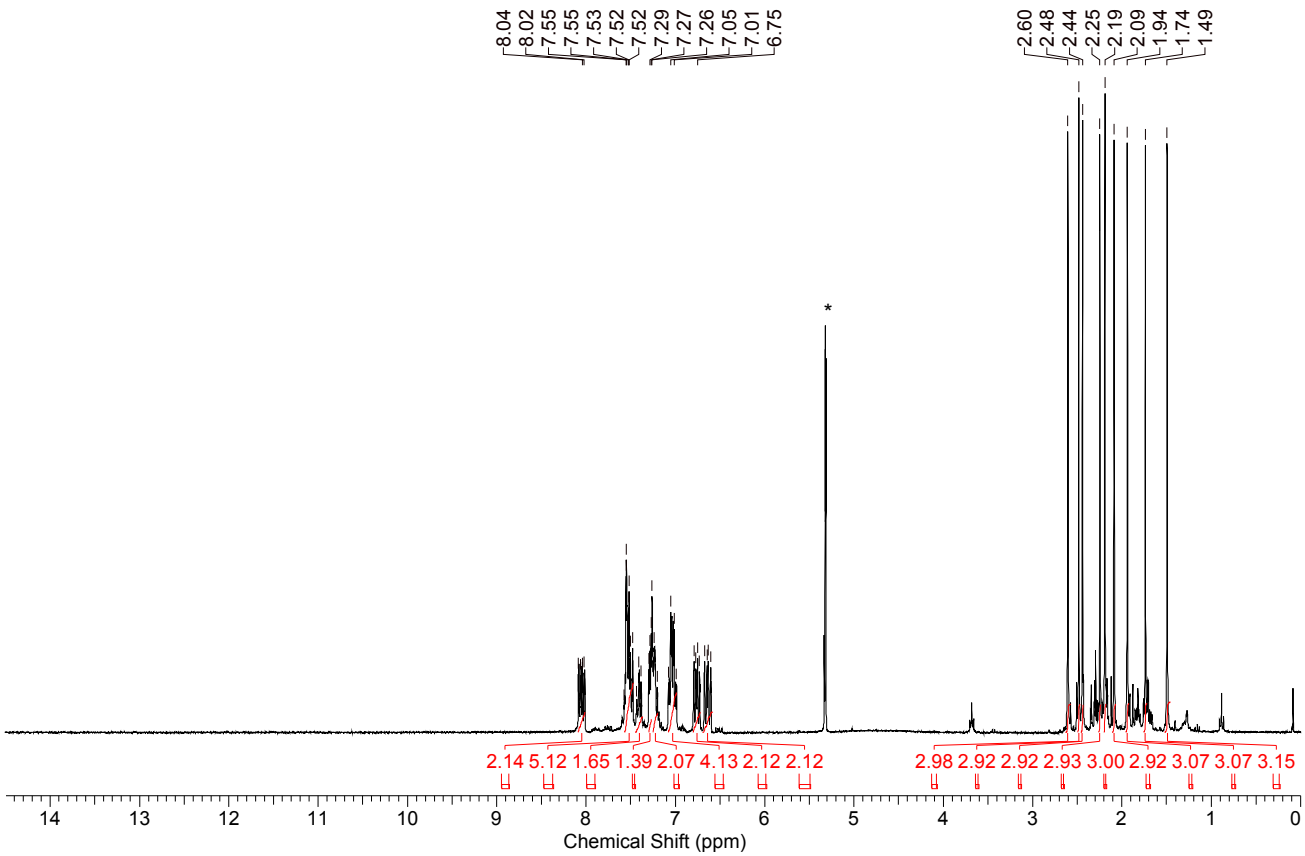

Figure S22. ^{1}H NMR of **2OO** in CD_2Cl_2 (*).

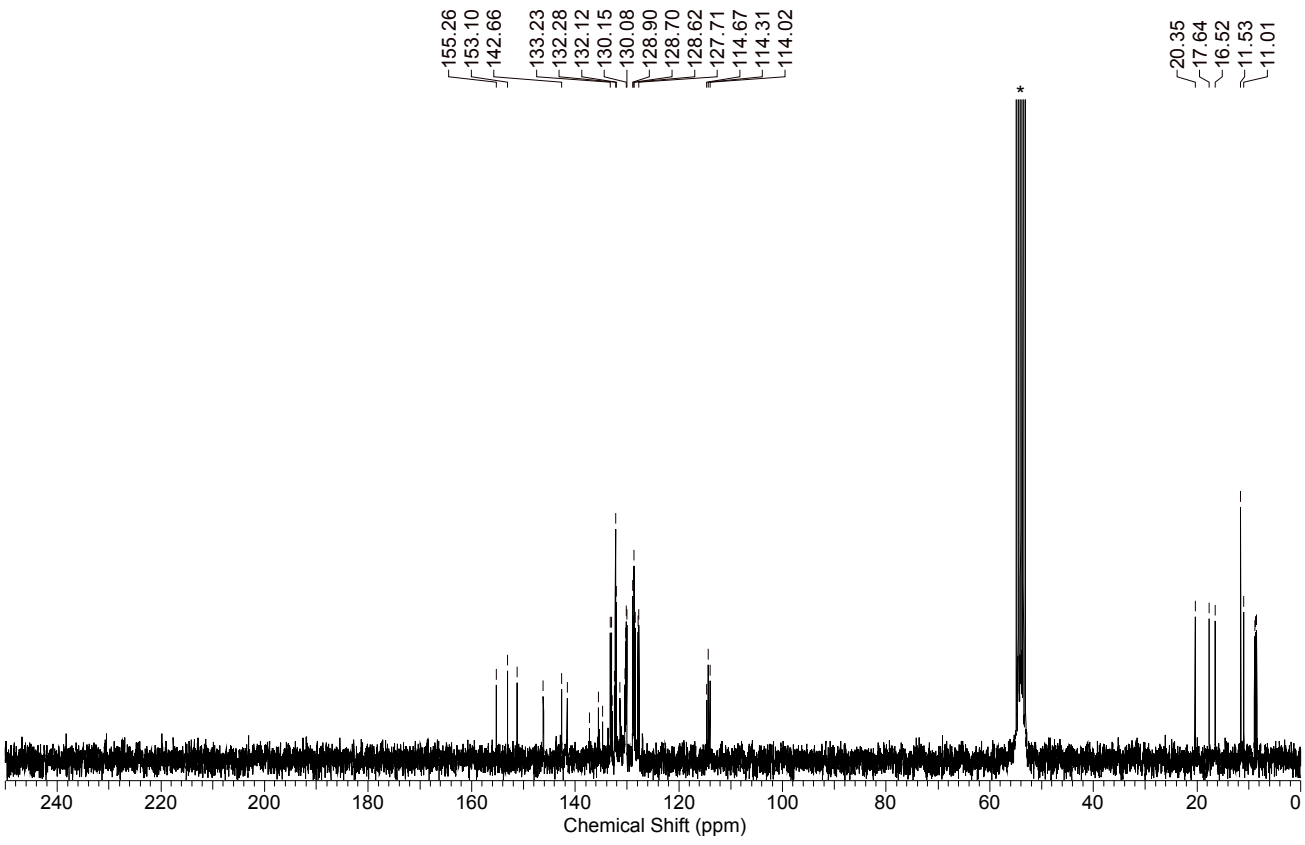

Figure S23. ^{13}C NMR of **2OO** in CD_2Cl_2 (*).

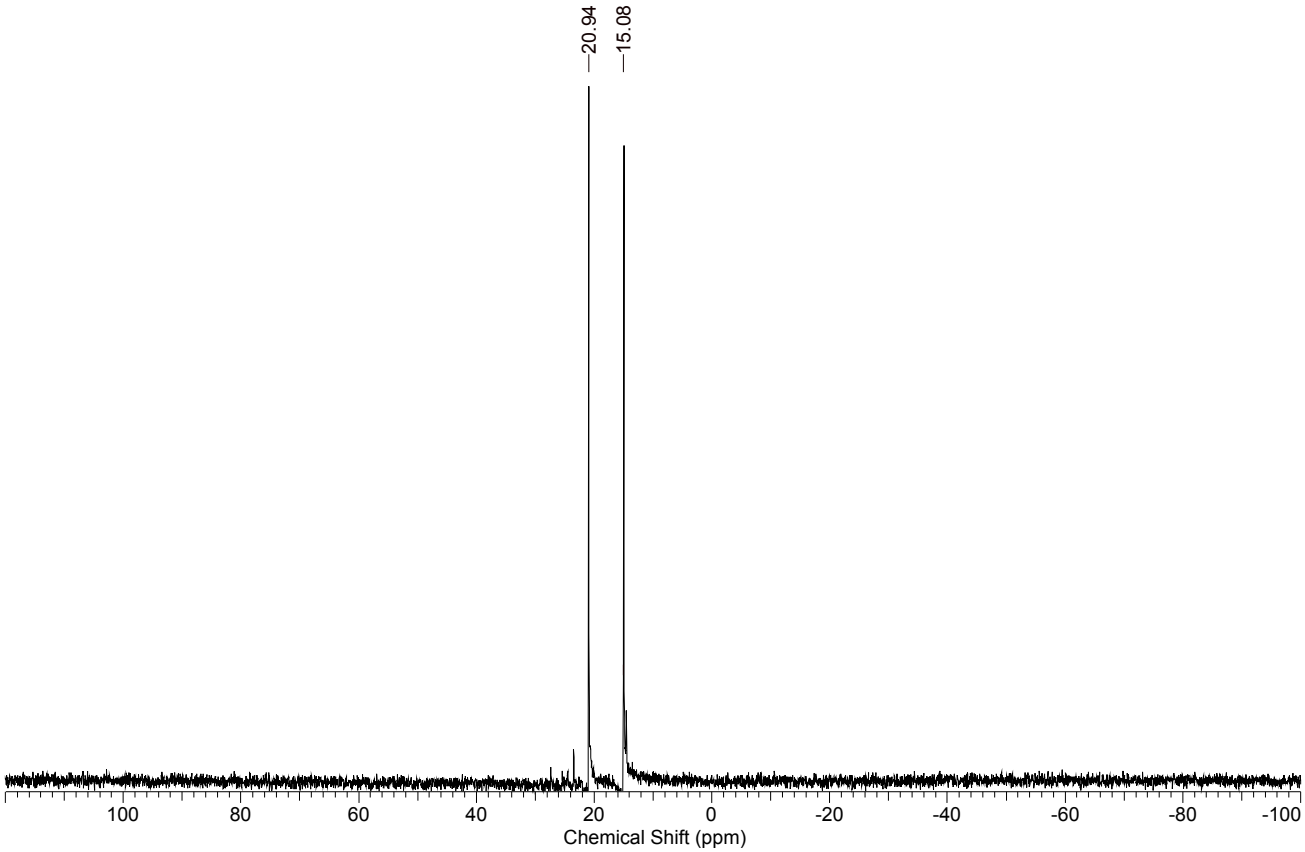

Figure S24. ^{31}P NMR of **2OO** in CD_2Cl_2.

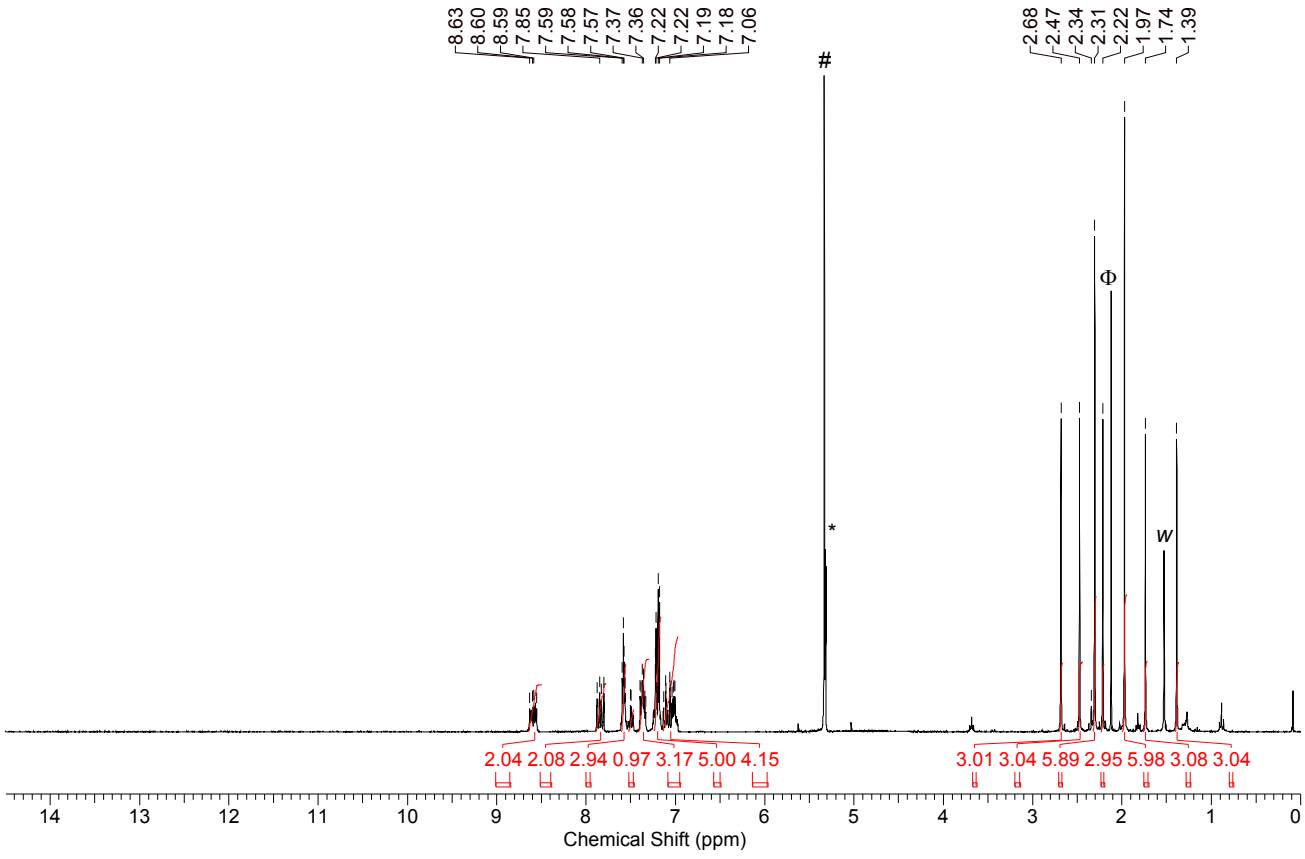

Figure S25. ^{1}H NMR of **2SS** in CD_2Cl_2 (*), # CH_2Cl_2, Φ acetone, *w* water.

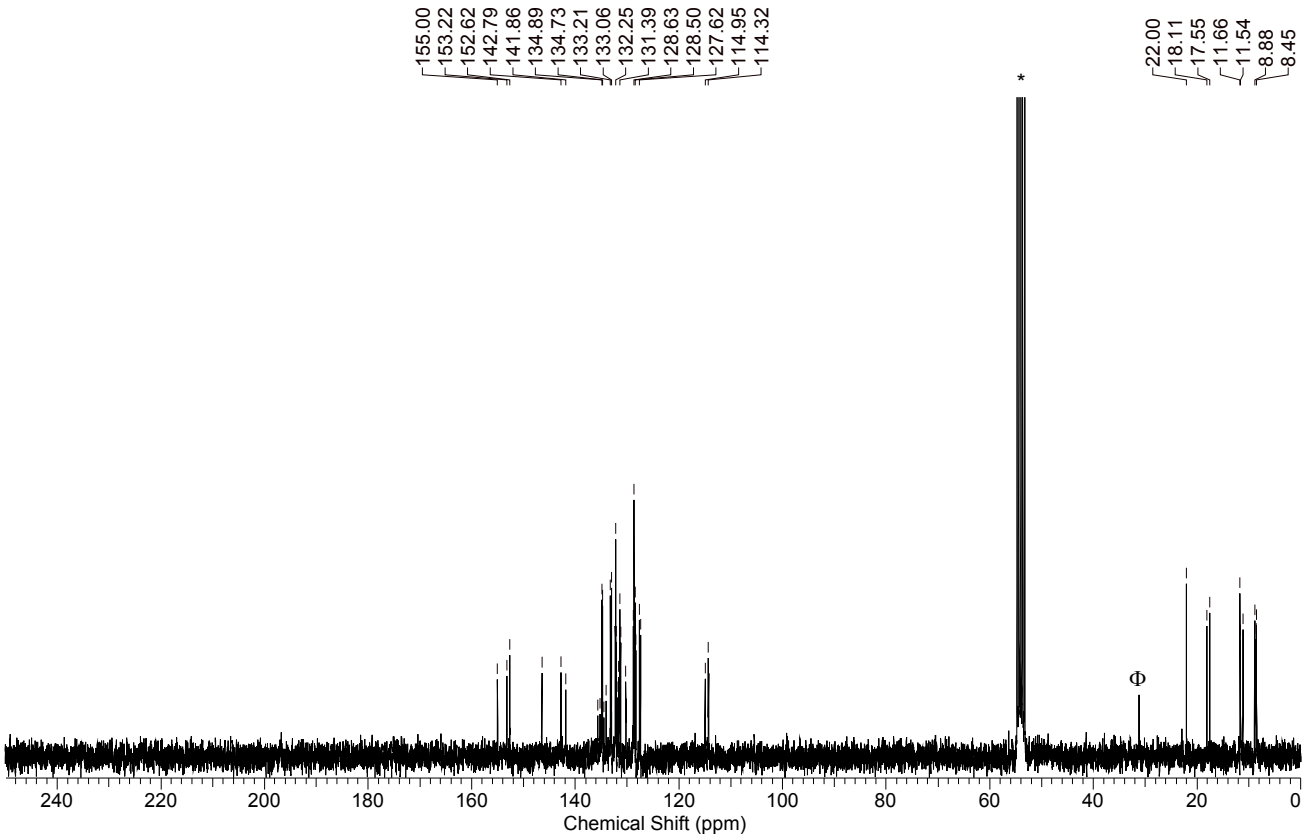

Figure S26. ^{13}C NMR of **2SS** in CD_2Cl_2 (*), Φ acetone.

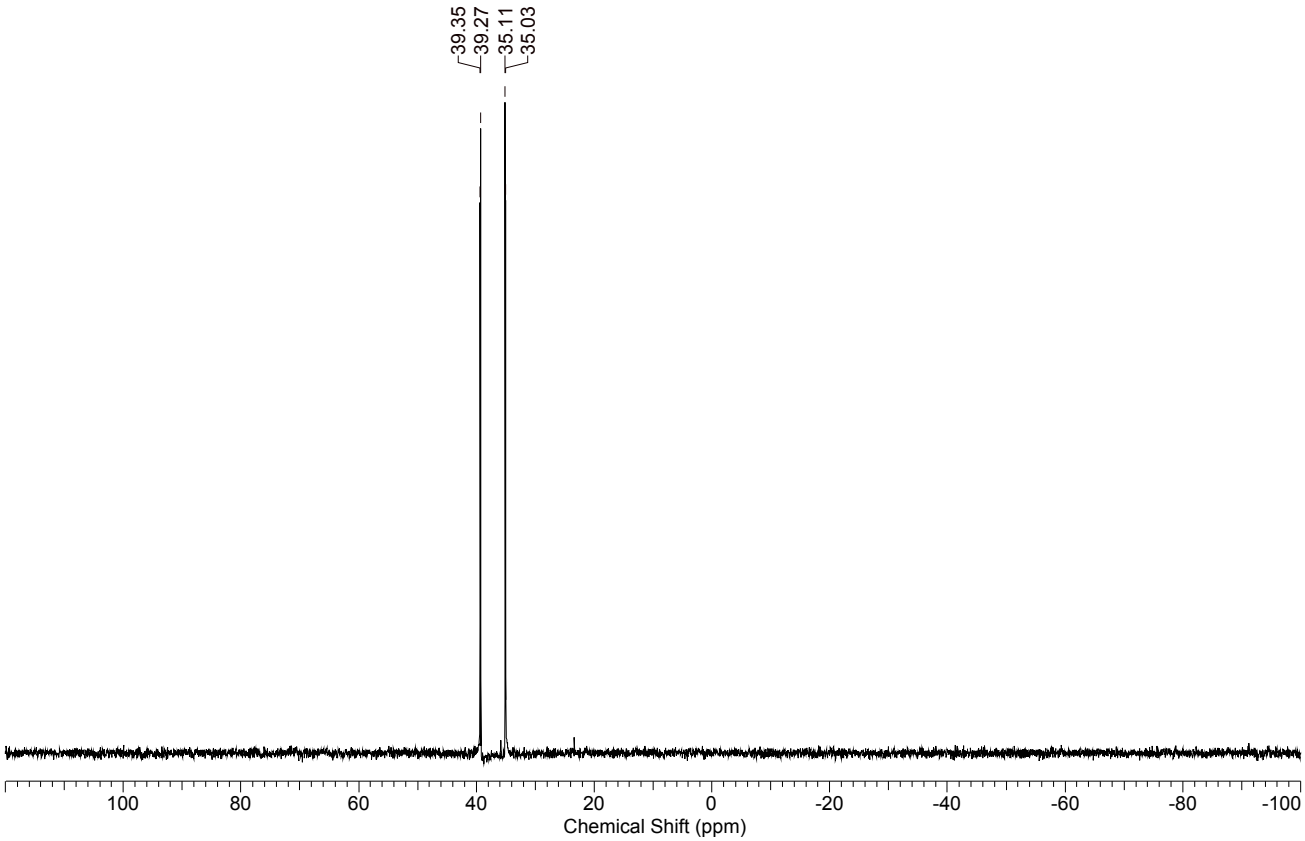

Figure S27. ^{31}P NMR of **2SS** in CD_2Cl_2.

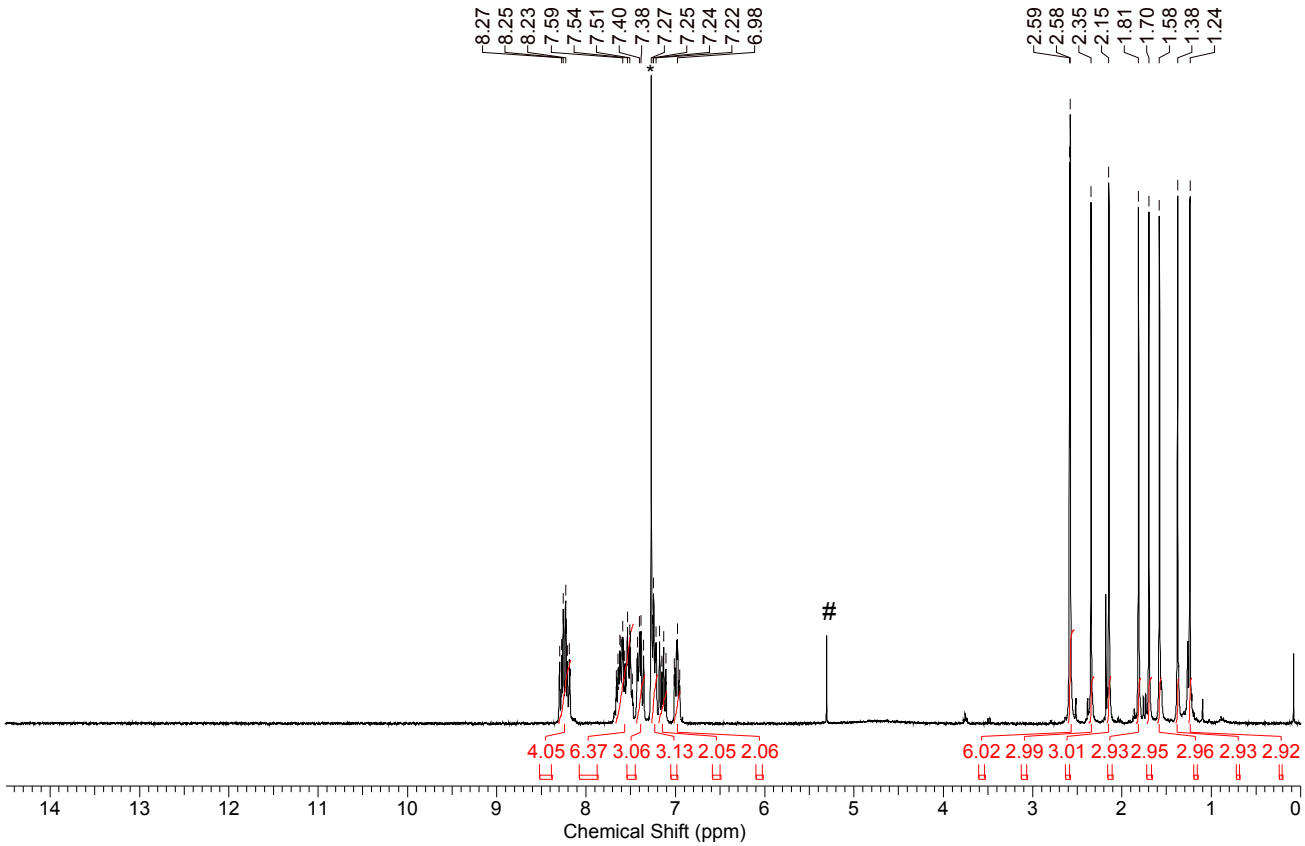

Figure S28. ^{1}H NMR of **3** in $CDCl_3$ (*), # CH_2Cl_2.

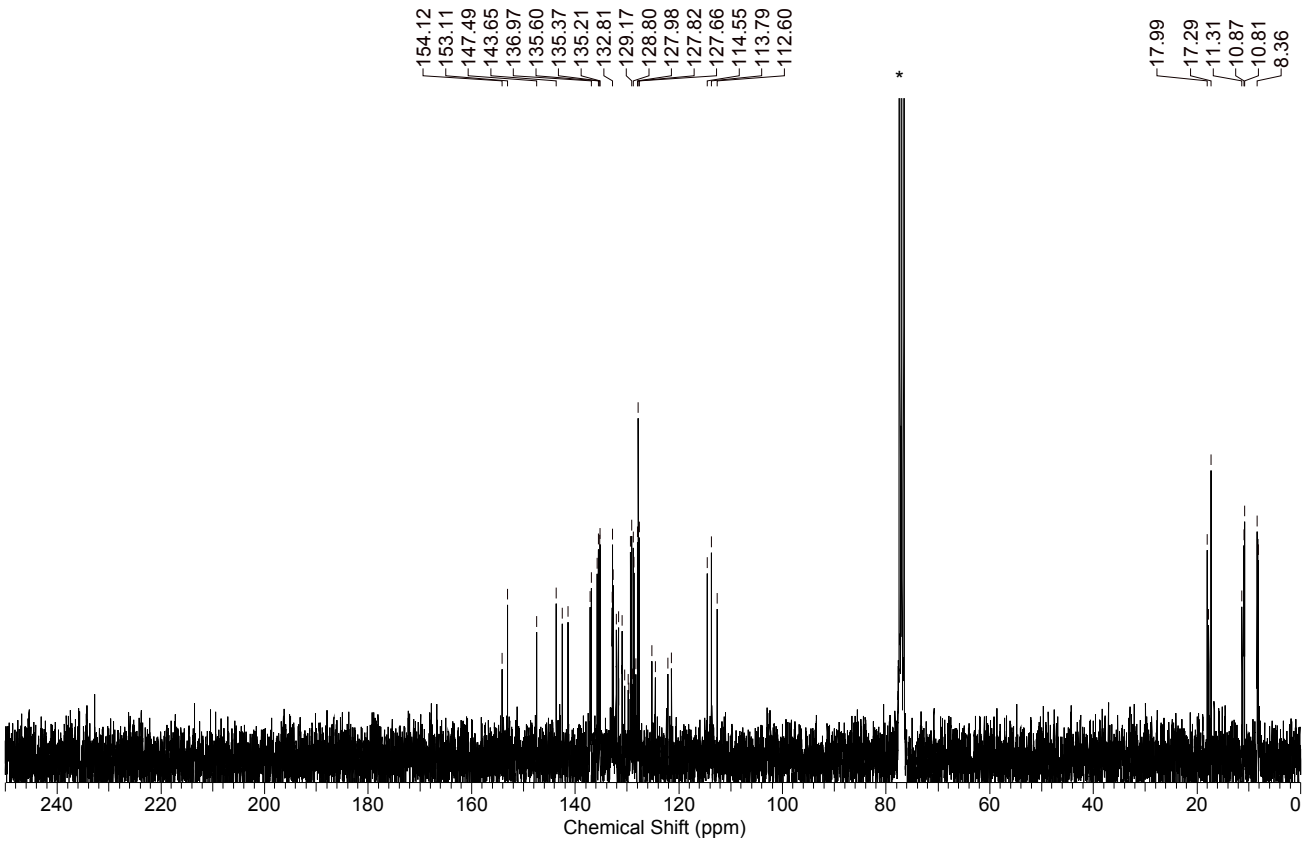

Figure S29. ^{13}C NMR of **3** in $CDCl_3$ (*).

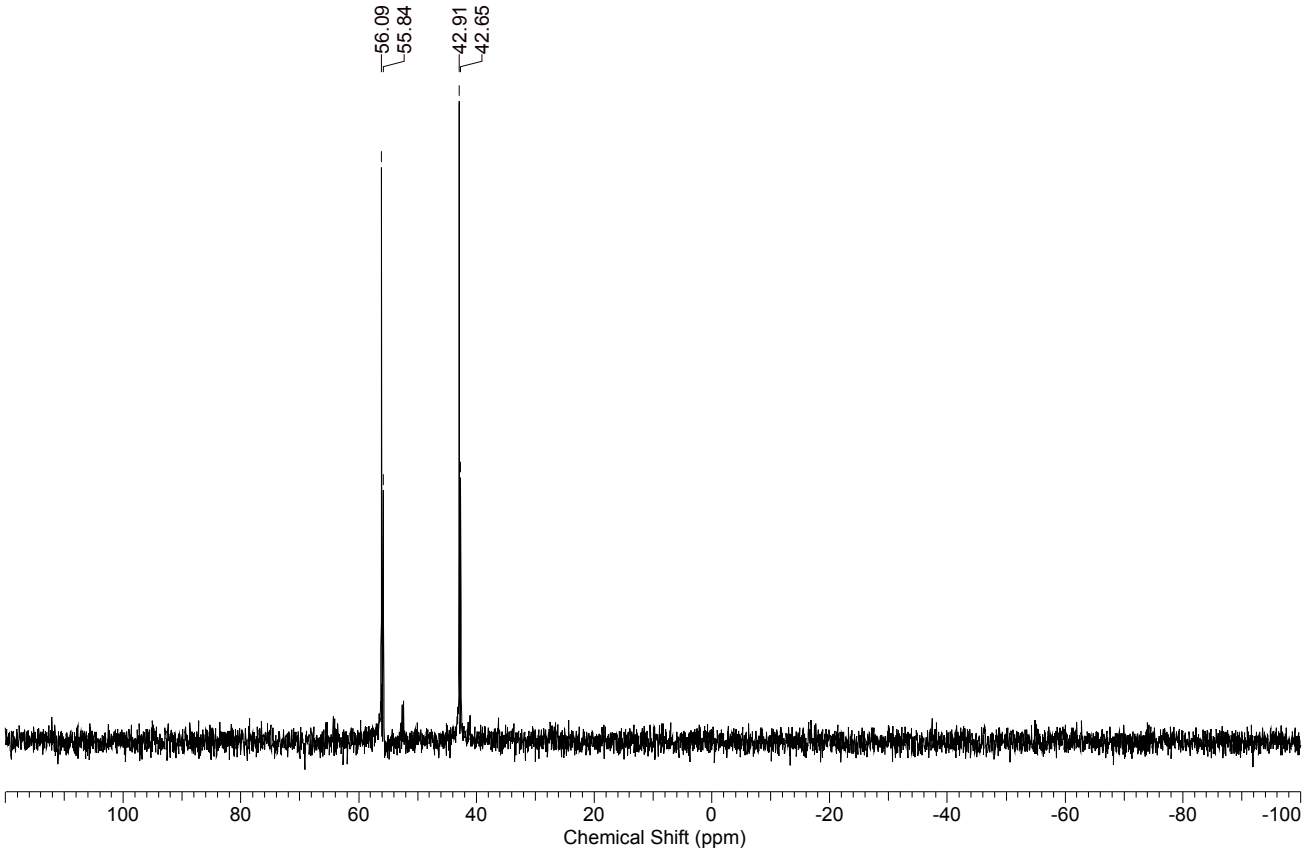

Figure S30. ^{31}P NMR of **3** in $CDCl_3$.

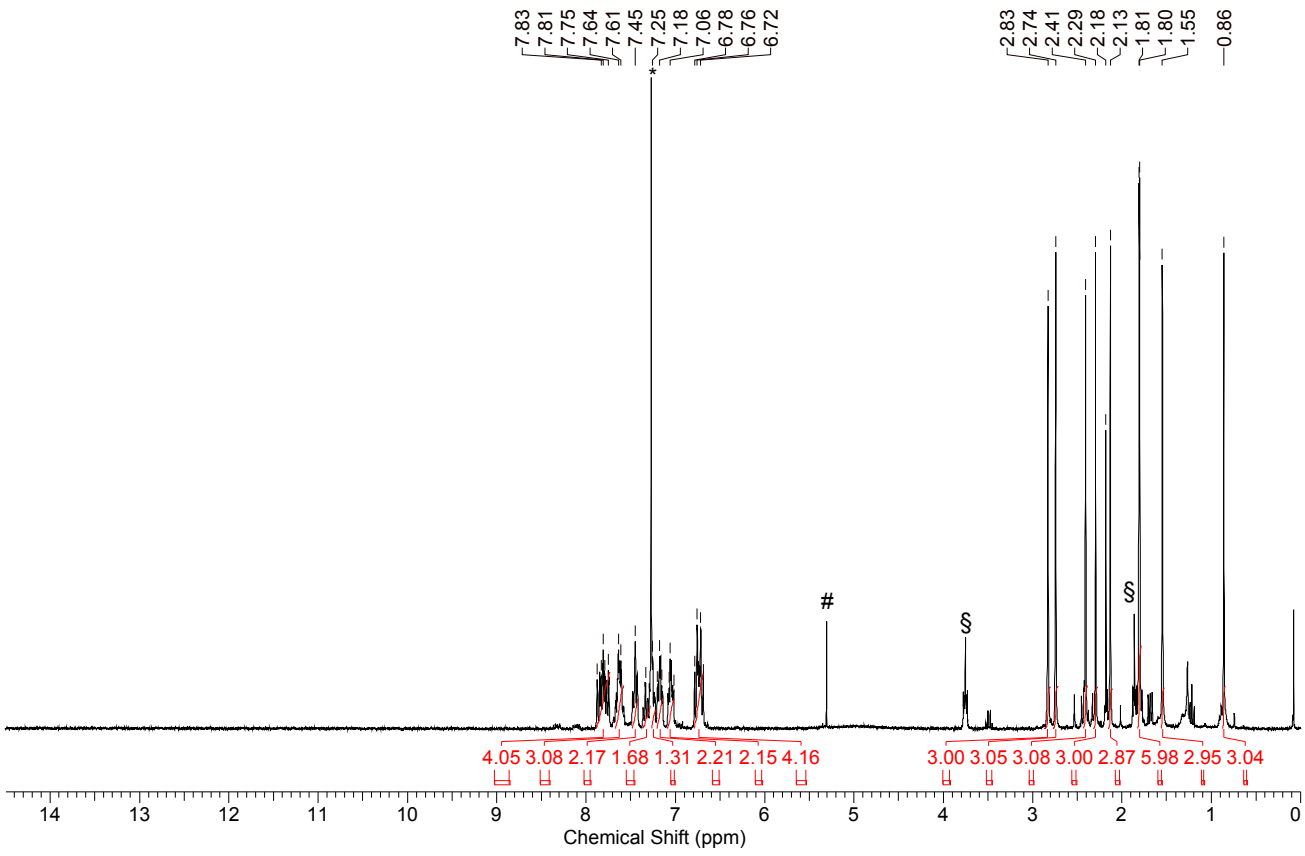

Figure S31. ^{1}H NMR of **3O** in $CDCl_3$ (*), # CH_2Cl_2, § thf.

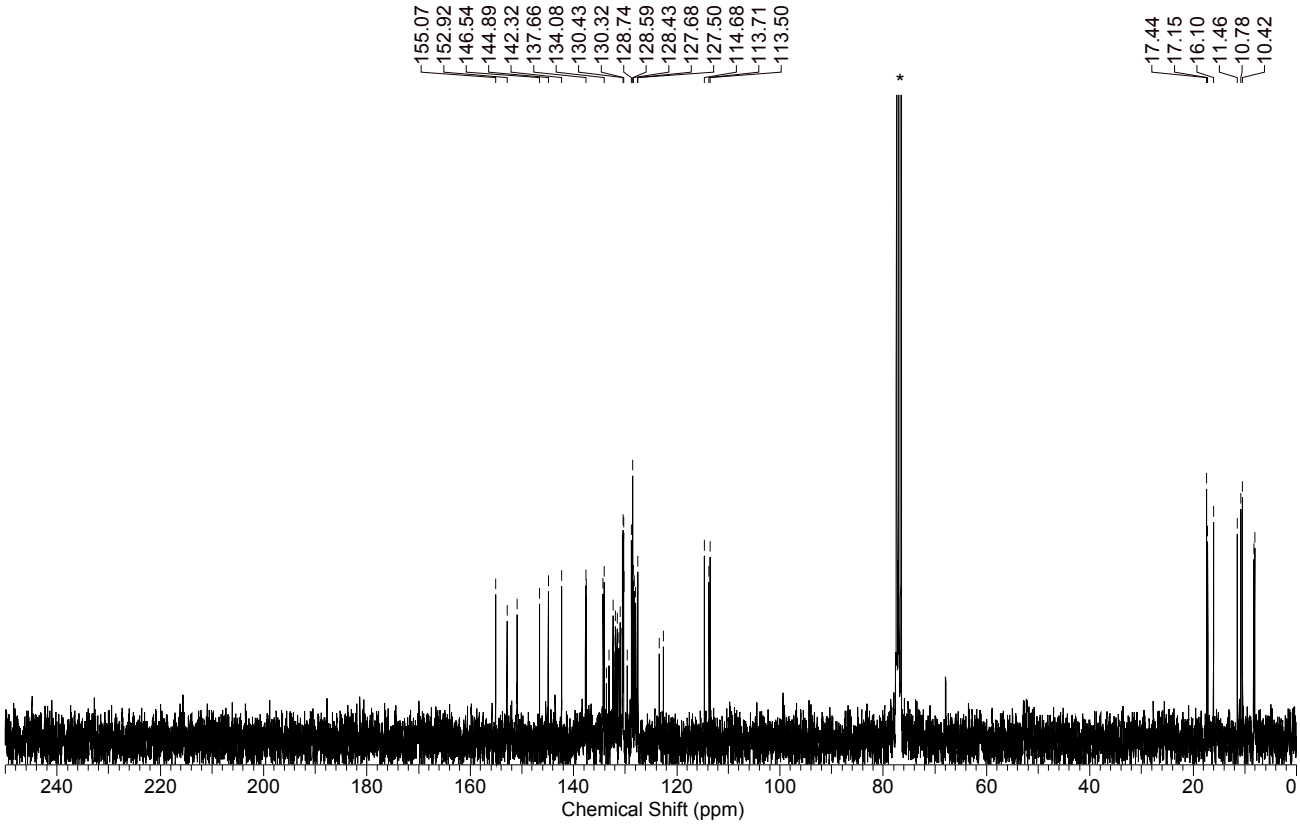

Figure S32. ^{13}C NMR of **3O** in $CDCl_3$ (*).

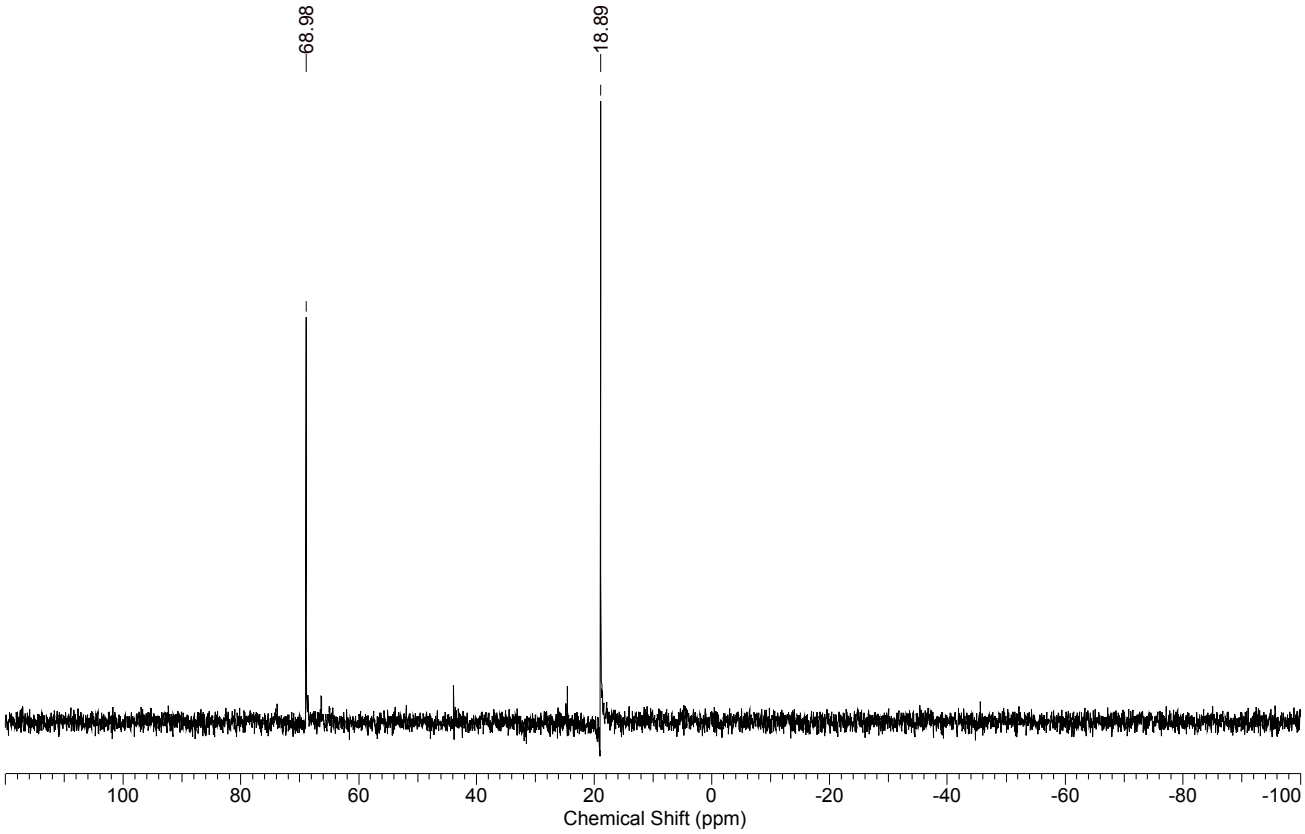

Figure S33. ^{31}P NMR of **3O** in $CDCl_3$.

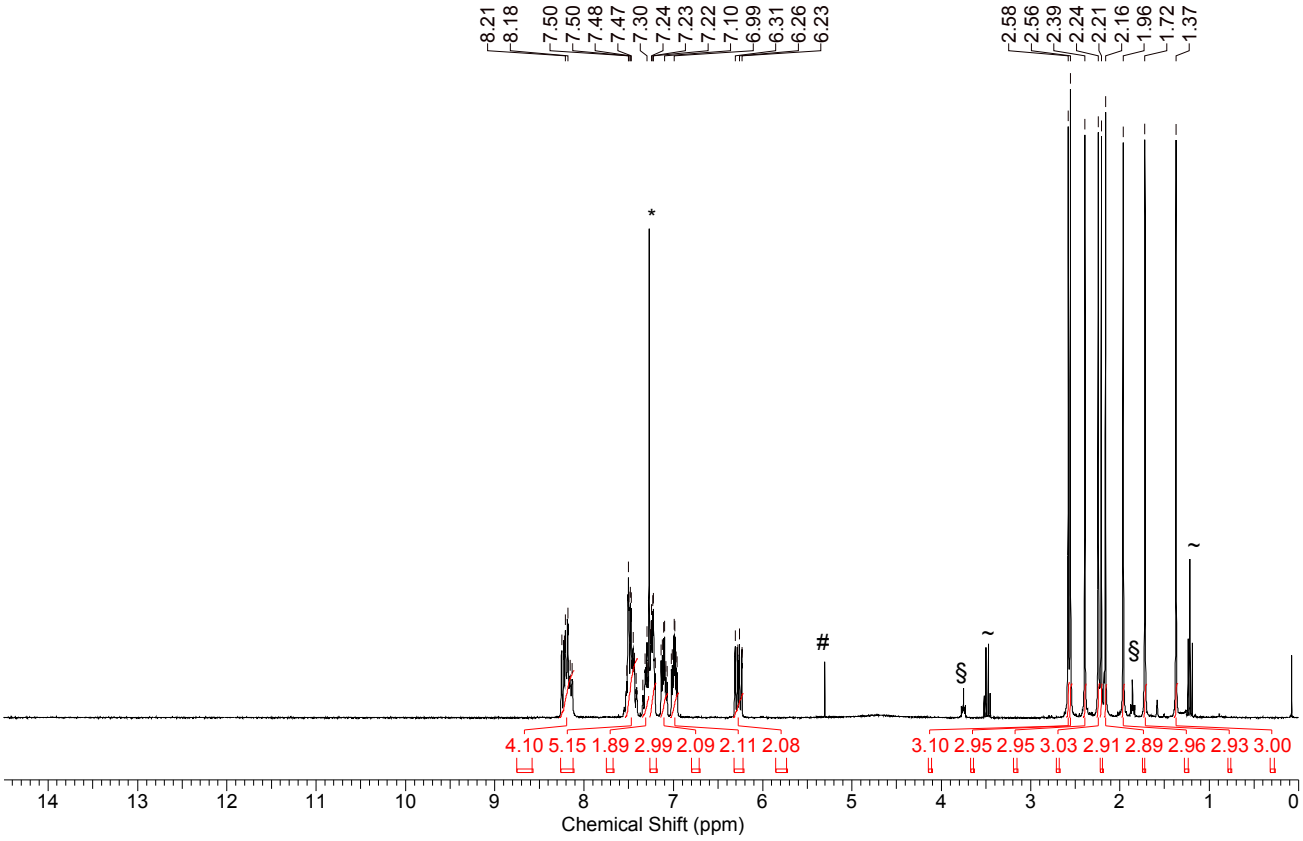

Figure S34. ^{1}H NMR of **3S** in $CDCl_3$ (*), # CH_2Cl_2, § thf, ~ diethyl ether.

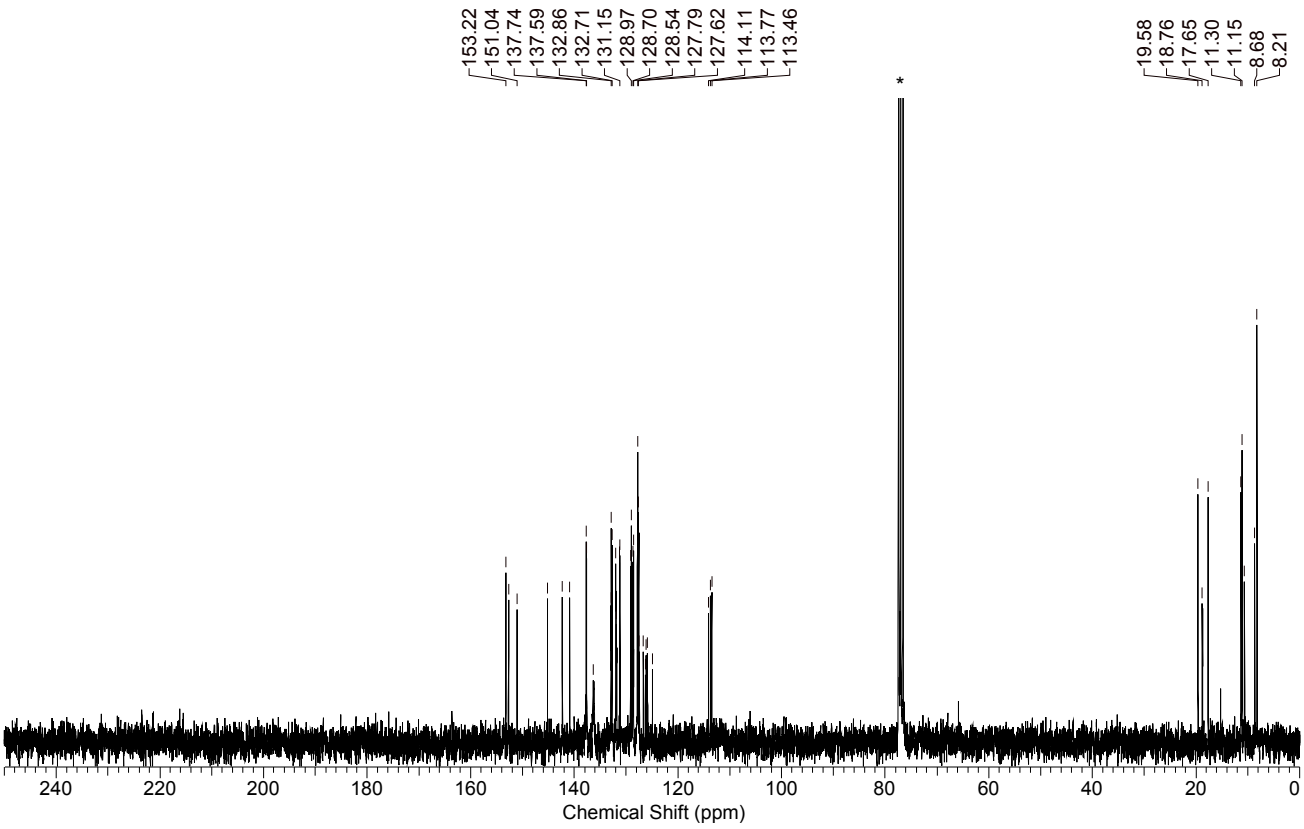

Figure S35. ^{13}C NMR of **3S** in $CDCl_3$ (*).

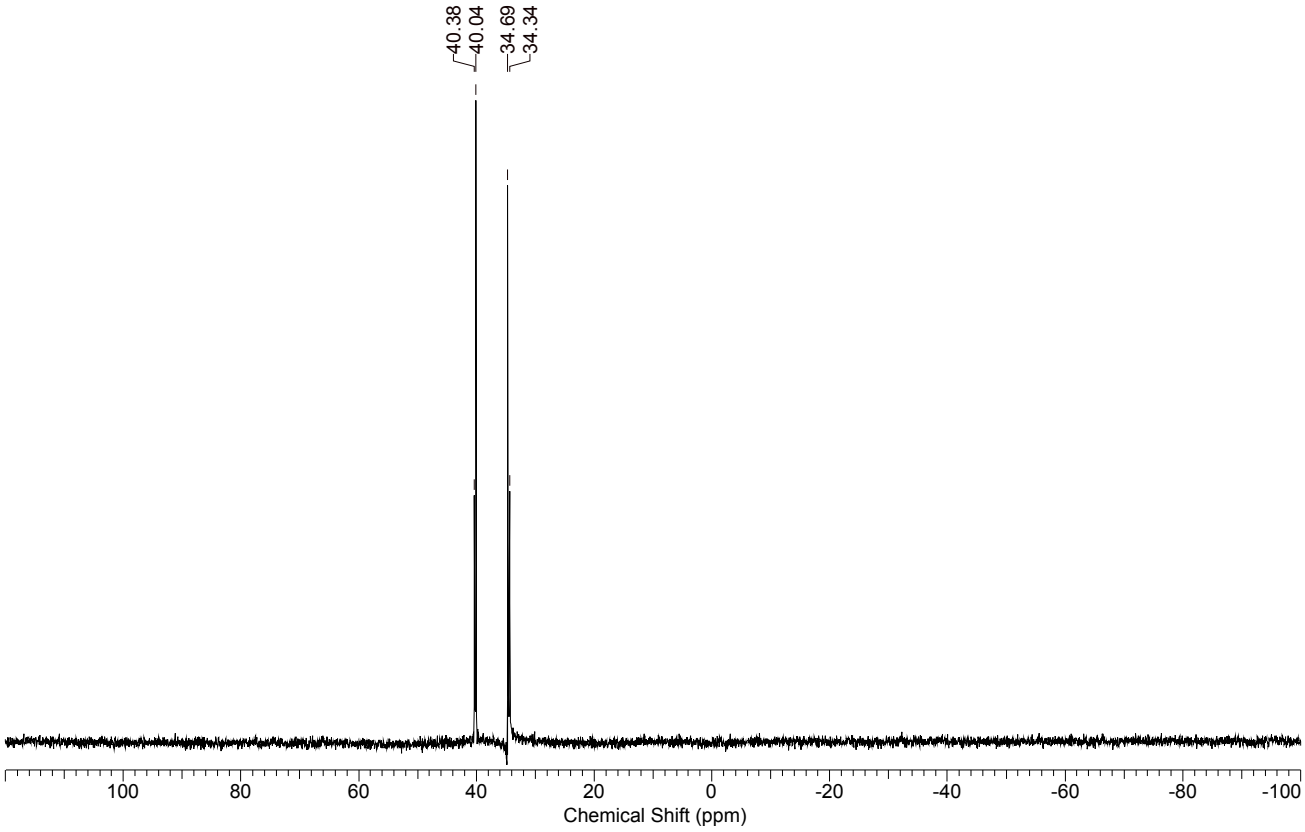

Figure S36. ^{31}P NMR of **3S** in $CDCl_3$.

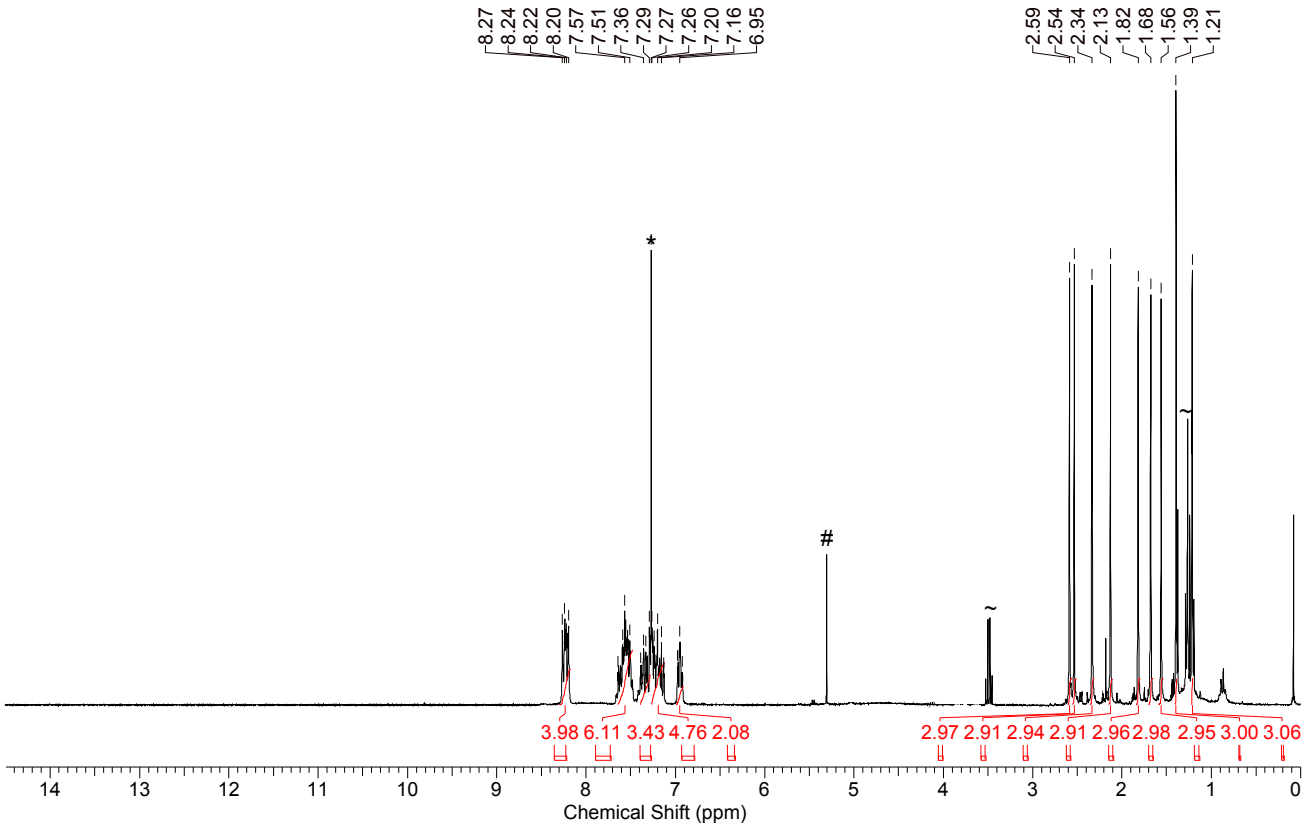

Figure S37. ^{1}H NMR of **4** in $CDCl_3$ (*), # CH_2Cl_2, ~ diethyl ether.

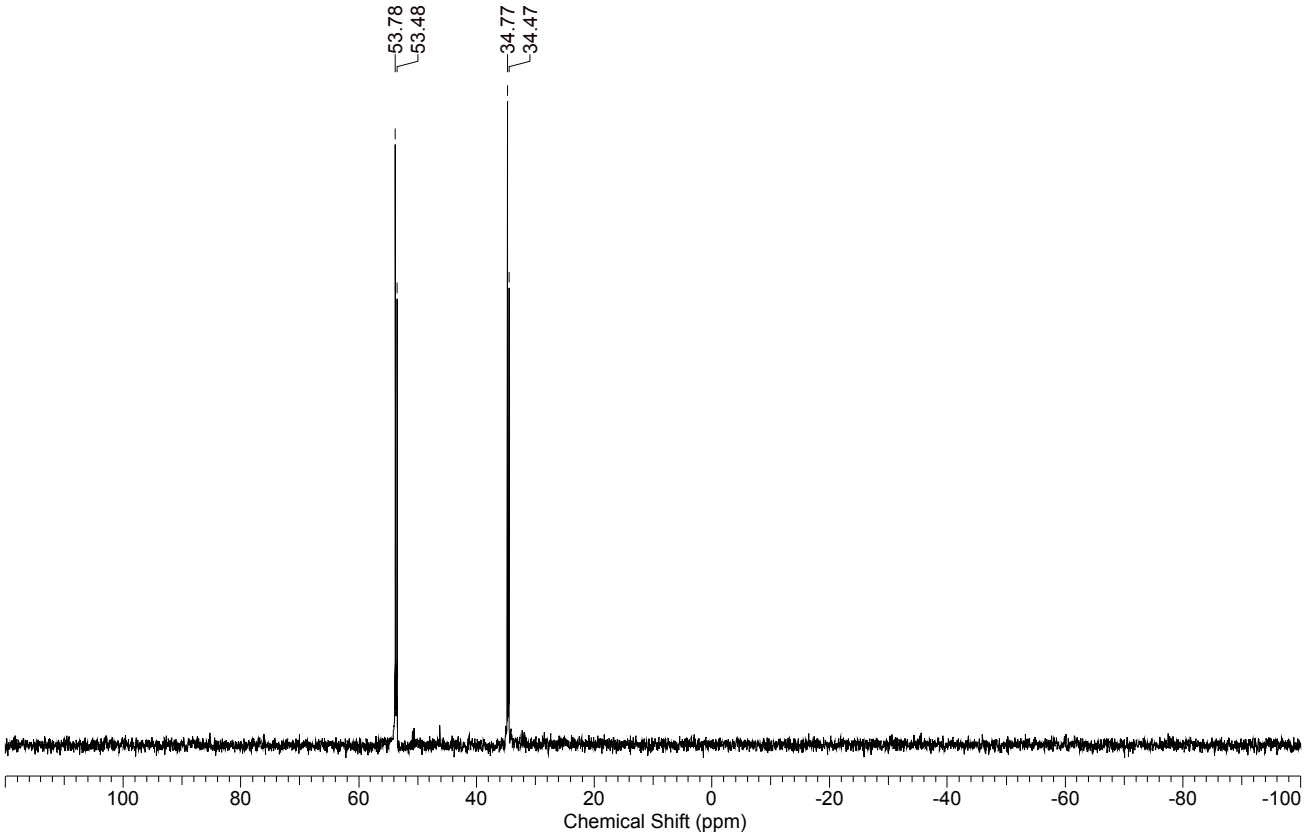

Figure S38. ^{31}P NMR of **4** in $CDCl_3$.

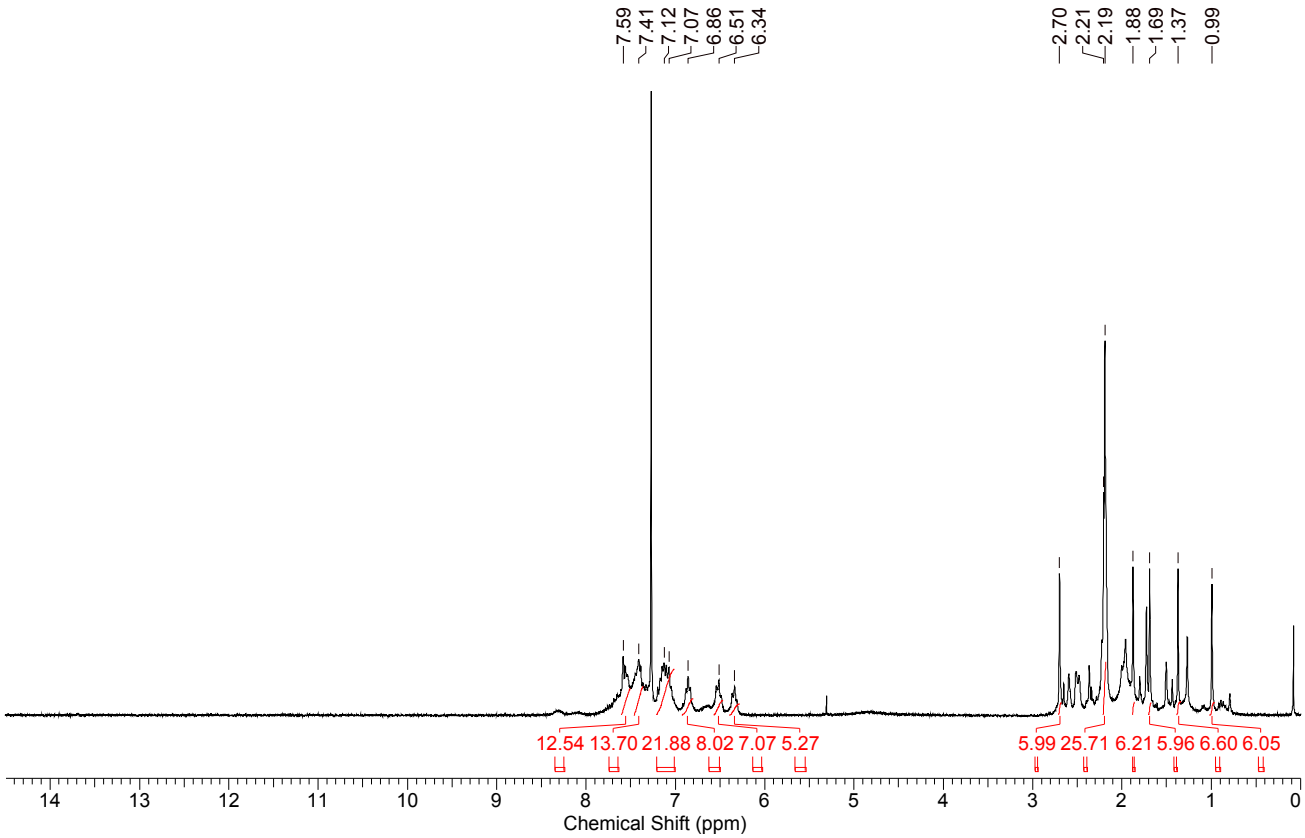

Figure S39. ^{1}H NMR of **5**-PF_6 in $CDCl_3$ (*), the spectrum quality is determined by solubility limitation.

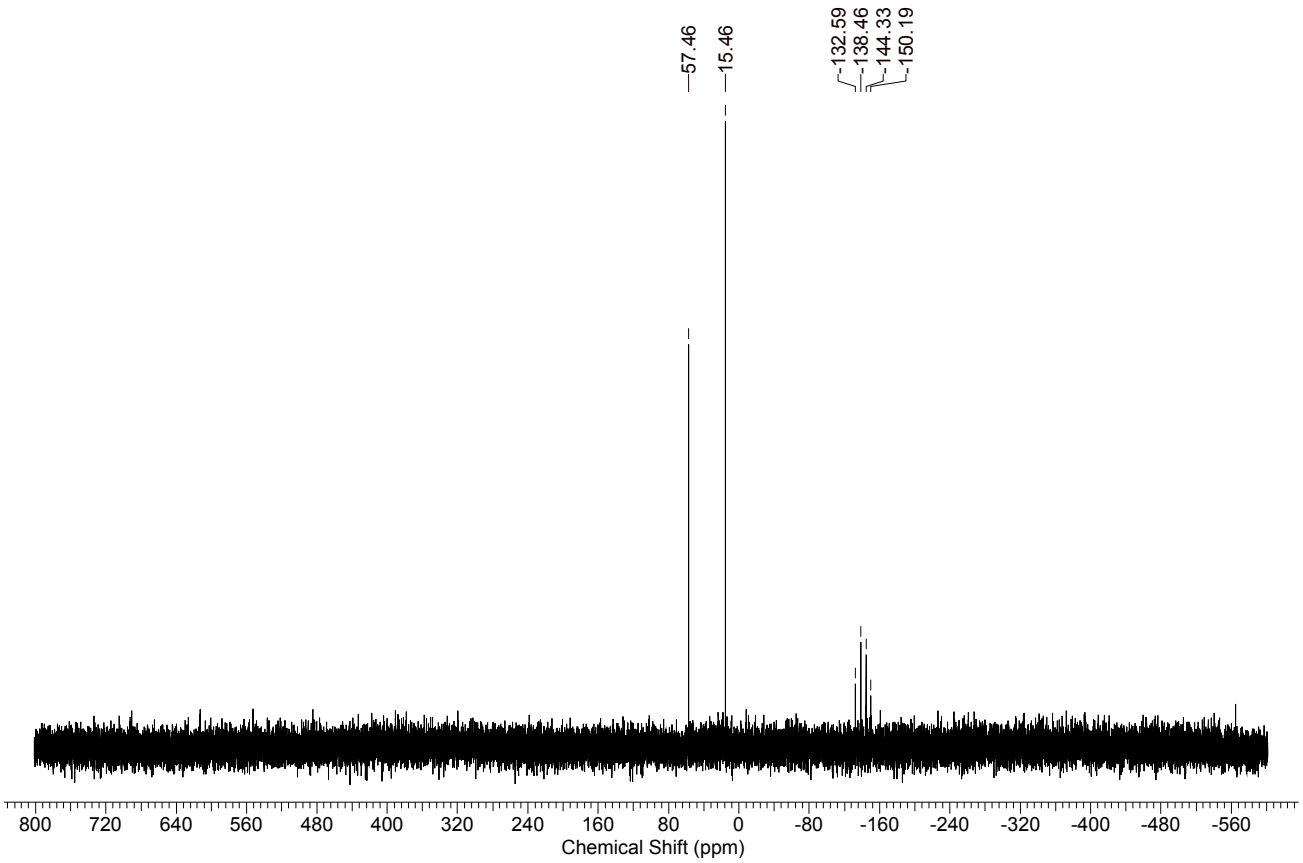

Figure S40. ^{31}P NMR of **5**-PF_6 in $CDCl_3$, the spectrum quality is determined by solubility limitation.

10. DFT Calculations

DFT calculations were carried out as closed shell calculations using the ORCA[S5] program package. Molecular geometries of **2**, **2O** and **2OO** were optimized without truncation and symmetry constraints in the gas phase using the BP86 functional.[S6] Quasi-relativistic effective core potentials of the Stuttgart/Cologne group were used for W (ECP60) and I (ECP46) in combination with a (8s7p6d2f1g)/[6s5p3d2f1g] basis set for W and a (4s5p)/[2s3p] basis set for I.[S7] Split valence triple ζ-basis sets (def2-TZVP) of the Ahlrich group were used for the other elements.[S8] In doing so a reasonable match between the calculated and the experimentally determined structures was achieved. Frequency calculations were performed to identify all stationary points as minima. The frontier Kohn-Sham orbitals of **2** are depicted with an isosurface value of 0.05 in Figure S41. For the calculations of the 5 lowest vertical singlet singlet transitions of **2**, **2O** and **2OO** TDDFT and the same functional/basis set combination were used. The visible absorption spectra in Figure S42 were obtained by assuming a peak half-width at half height of 2500 cm^{-1}.

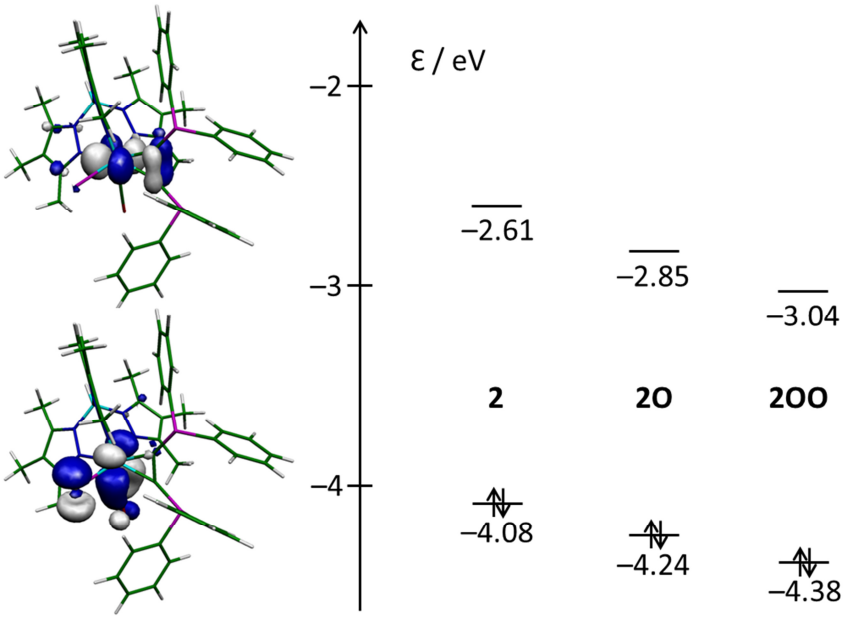

Figure S41. Representation of the frontier Kohn-Sham orbitals of **2** (HOMO, LUMO) and associated orbital energy diagram for **2**, **2O** and **2OO**.

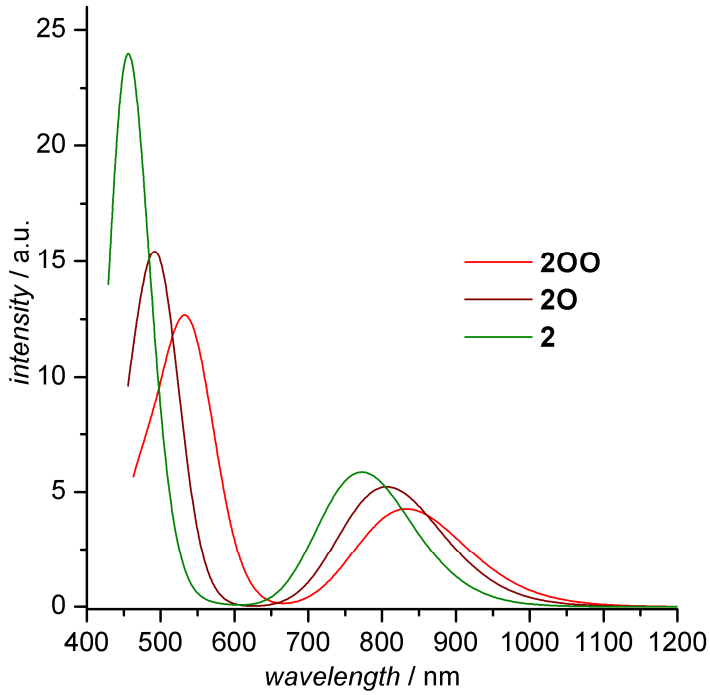

Figure S42. Calculated visible absorption spectra of **2** (λ_{max} = 773 nm), **2O** (λ_{max} = 807 nm) and **2OO** (λ_{max} = 833 nm).

11. References

(S1) Frohnapfel, D. S.; Reinartz, S.; White, P. S.; Templeton, J. L. *Organometallics* **1998**, *17*, 3759–3769.

(S2) (a) Templeton, J. L. *Adv. Organomet. Chem.* **1989**, *29*, 1–100. (b) M. Bartlett, I.; Carlton, S.; G. Connelly, N.; J. Harding, D.; D. Hayward, O.; Guy Orpen, A.; D. Ray, C.; H. Rieger, P. *Chem. Commun.* **1999**, 2403–2404. (c) Adams, C. J.; Bartlett, I. M.; Carlton, S.; Connelly, N. G.; Harding, D. J.; Hayward, O. D.; Orpen, A. G.; Patron, E.; Ray, C. D.; Rieger, P. H. *Dalton Trans.* **2007**, 62–72.

(S3) Jiao, J.; Long, G. J.; Rebbouh, L.; Grandjean, F.; Beatty, A. M.; Fehlner, T. P. *J. Am. Chem. Soc.* **2005**, *127*, 17819–17831.

(S4) Helmdach, K.; Ludwig, S.; Villinger, A.; Hollmann, D.; Kösters, J.; Seidel, W. W. *Chem. Commun.* **2017**, *53*, 5894–5897.

(S5) a) Neese, F. *ORCA – An ab initio, DFT, and semi-empirical SCF-MO package* **2012**, version 3.0.2; b) Neese, F. The ORCA program system, *Wiley Interdiscip. Rev.: Comput. Mol. Sci.* **2012**, *2*, 73–78.

(S6) a) Becke, A. D. *J. Chem. Phys.* **1986**, *84*, 4524–4529; b) Perdew, J. P. *Phys. Rev. B* **1986**, *33*, 8522.

(S7) a) Andrae, D.; Häußermann, U.; Dolg, M.; Stoll, H.; Preuß, H. *Theor. Chim. Acta* **1990**, *77*, 123–141; b) Martin, J. M. L.; Sundermann, A. *J. Chem. Phys.* **2001**, *114*, 3408–3420; c) Bergner, A.; Dolg, M.; Küchle, W.; Stoll, H.; Preuß, H. *Mol. Phys.* **1993**, *80*, 1431–1441.

(S8) Weigend, F.; Ahlrichs, R. *Phys. Chem. Chem. Phys.* **2005**, *7*, 3297–3305.